Electronic Supplementary Material (ESI) for RSC Advances
This journal is © The Royal Society of Chemistry 2015

Supporting Information

A Practical Anodic Oxidation of Aminofurazans to Azofurazans: an environmentally friendly route

Aleksei B. Sheremetev,*[a] Boris V. Lyalin,[a] Andrei M. Kozeev,[a] Nadezhda V. Palysaeva,[a] Marina I. Struchkova,[a] and Kyrill Yu. Suponitsky[b]

[a] *N. D. Zelinsky Institute of Organic Chemistry, Russian Academy of Sciences, 119991 Moscow, Russian Federation. Fax: +7 499 135 5328; e-mail: sab@ioc.ac.ru*
[b] *A. N. Nesmeyanov Institute of Organoelement Compounds, Russian Academy of Sciences, 119991 Moscow, Russian Federation.*

Contents **Page**

Voltammetry. The electro-chemical tests were carried out using a Econix potentiostat (scan rate error 1.0%, potential setting 0.25 mV) in a three-electrode cell setup with electrodeposited NiOOH[48] on Ni foil (d = 1.0 mm) substrate or a glassy-carbon electrode (d = 1.7 mm) as working electrode, platinum (Pt) wire as counter electrode, and a saturated calomel electrode (SCE) as reference electrode.

Recording of voltammetric curves with scanning potential to the positive range up to background electrolyte discharge oxidation peaks does not show. Upon immersion of Ni electrode in alkaline media and electrode polarization through thirtyfold pulsing (duration time of each pulse – 3 s) with potential of background electrolyte discharge (-1300 and +700 mV), a layer of NiOOH immediately forms on the electrode surface. After that on the oxidation curves a reversible peak corresponding to Ni^{2+}/Ni^{3+} pair[49] was observed (Figure S1a). The forward and the reverse peaks currents are linearly dependent on the square root of the potential scanning rate (Figure S1b).

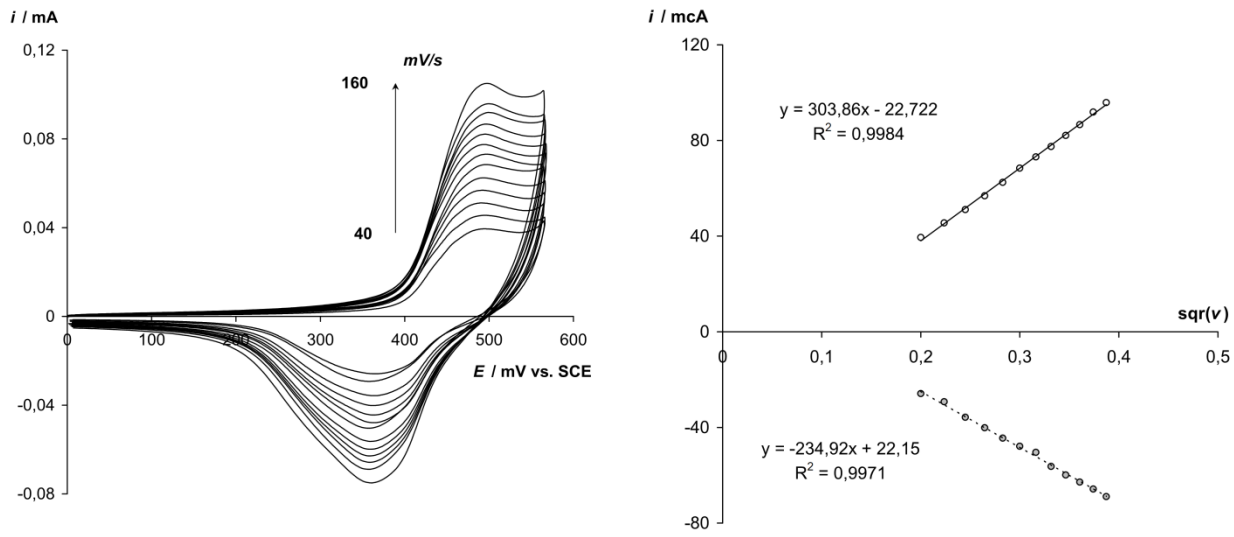

Figure S1. (***a***) CVs of Ni/NiOOH in 0.2 M NaOH at scan rates of 40, 50, 60, 70, 80, 90, 100, 110, 120, 130, 140, 150 and 160 mV s^{-1}; (**b**) the plots of peak current versus square root of scan rate.

The tested solutions were thermostated at 25±0.5 °C. Deaeration of solutions was performed by passing argon. To prevent contact between the solution surface and the ambient air during the experiment, argon was constantly fed to the cell's free space above the solution surface. In a typical case, 5 ml of a solution was utilized and the solution was agitated vigorously with argon before recording each CV curve.

Oxidation product, the azofurazan **9a**, is electron-deficient compound with rich π-system. As a result, its high electron affinity and reduction may be expected in relatively moderate potential range. Unfortunately, a study of the azo compound electroreduction is hampered by its poor solubility under the experimental conditions (< 1 mmol L^{-1}). On the CV-curves recorded with the potential scanning in the negative direction using Ni or Ni/NiOOH working electrode, appearance of reduction peaks was not identified after addition of compound **9a** to the solution (Fig. S2). Nevertheless, on glassy-carbon working electrode under the same conditions, appearance of reversible electroreduction peak at -0.37 V was detected, that probably correspond to formation of a radical anion from compound **9a**. It should be noted, that under electrolysis conditions discharge on the cathode in alkaline solution occurs and accomplished by the hydrogen formation. However, the concentration of water is more than three orders of magnitude higher than the concentration of the azo compound **9**. In this regard, the need to use double amount of electricity to achieve maximum yield of the product **9a** is probably due to losses due to electrolysis of water.

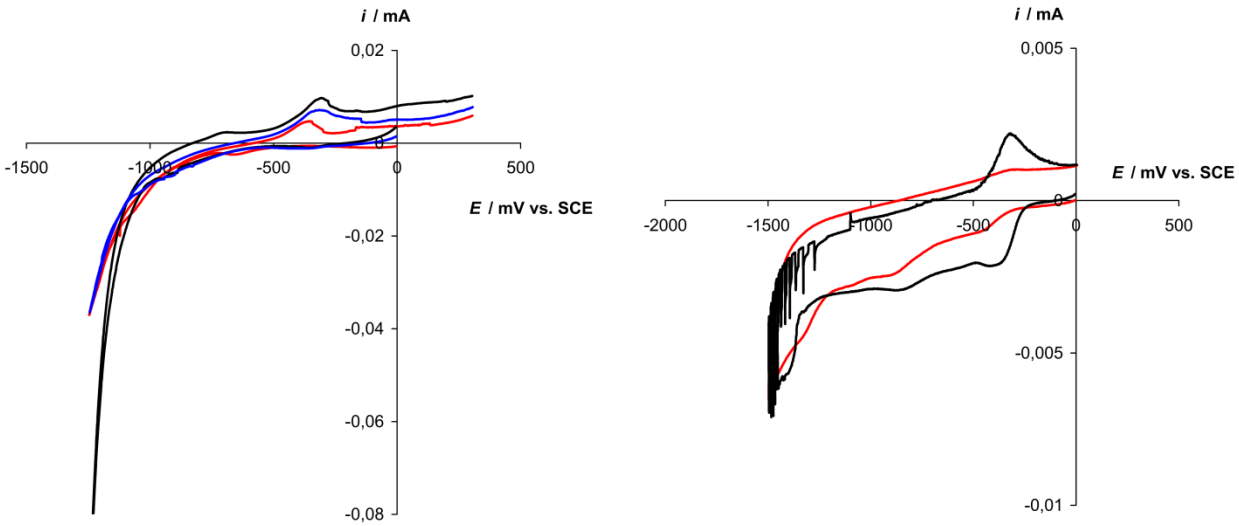

Figure S2. (a) CVs in 0.2 M NaOH, scan rate 50 mV s^{-1}. (red) Ni/NiOOH working electrode; (blue) Ni/NiOOH working electrode, 0.5 mmol L^{-1} **9a**; (black) Ni working electrode, 0.5 mmol L^{-1} **9a**. (b) (red) CVs in 0.2 M NaOH, scan rate 50 mV s^{-1}, glassy-carbon working electrode; (black) with addition of compound **9a** (0.5 mmol L^{-1}).

Electrochemical mechanisms. It is well-documented, upon immersion in alkaline media, a layer of $Ni(OH)_2$ forms on the Ni electrode, Eq. (1 and 2). This $Ni(OH)_2$ layer undergoes a Ni^{2+}/Ni^{3+} redox process, Eq. (3). The NiOOH catalyst mediates the amine oxidation reaction, Eq. (4). At the oxidation process, the active electrode surface is chemically reduced to the Ni^{2+} oxidation state by the amine which is chemically oxidized to azo compound. The inactive $Ni(OH)_2$ will be electrochemically oxidized to NiOOH thus regenerating the catalyst for further oxidation of the amine.

Anode :

$$4Ni \rightarrow 4Ni^{2+} + 8e- \quad (1)$$

$$4Ni^{2+} + 8OH^- \rightarrow 4Ni(OH)_2 \quad (2)$$

$$4Ni(OH)_2 + 4OH^- \rightarrow 4NiOOH + 4H_2O + 4e- \quad (3)$$

$$4NiOOH + 2R\text{-}NH_2 \rightarrow 4Ni(OH)_2 + R\text{-}N{=}N\text{-}R \quad (4)$$

Cathode :

$$12H_2O + 12e- \rightarrow 6H_2 + 12OH^- \quad (5)$$

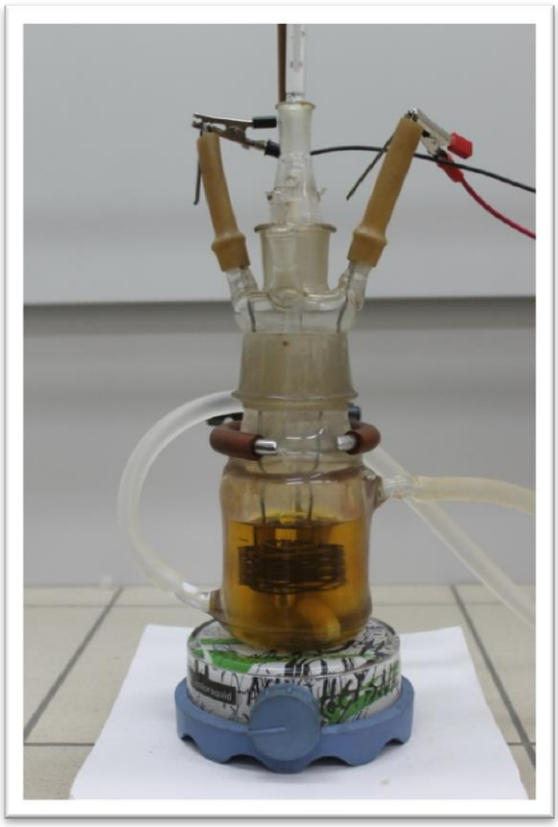

Figure S3. General view of the apparatus. anodic oxidation of aminofurazans to azofurazans.

Single Crystal X-ray Diffraction Study of compounds 9d and 11

X-ray experiments were carried out using SMART APEX2 CCD (λ(Mo-Kα)=0.71073 Å, graphite monochromator, *ω*-scans) at 100K. Collected data were analized by the SAINT and SADABS programs incorporated into the APEX2 program package.[50] All structures were solved by the direct methods and refined by the full-matrix least-squares procedure against F^2 in anisotropic approximation. The H(C) positions were calculated, and included in the refinement within isotropic approximation using the riding model with the $1.2U_{eq}(C)$, where $U_{eq}(C)$ are the equivalent thermal parameters of the parent carbon atoms. The refinement was carried out with the SHELXTL program.[51] The details of data collection and crystal structures refinement are summarized in Table S1. Crystallographic information files are available from the Cambridge Crystallographic Data Center (CCDC) upon request (http://www.ccdc.cam.ac.uk, deposition numbers 1007707–1007708).

Table S1. Crystallographic data for **9d** and **11**.

Parameter	**9d**	**11**
Empirical formula	$C_{10}H_{10}N_6O_2$	$C_4N_{10}O_2$
Fw	246.24	220.14
Crystal system	Orthorhombic	Orthorhombic
Space group	*Pbca*	$P2_12_12_1$
a, Å	7.6654(5)	8.1050(9)
b, Å	9.6969(6)	8.5614(9)
c, Å	15.2346(10)	11.3382(12)
V, Å^3	1132.40(13)	786.76(15)
Z	4	4
d_{calc}, g·cm^{-3}	1.444	1.859
μ, mm^{-1}	0.107	0.156
F(000)	512	440
θ range, deg.	3.64 – 32.00	2.98 – 31.13
reflections collected	14832	11319
independent reflections	1967	1475
R_{int}	0.0261	0.0839
refined parameters	82	145
Completeness to theta θ, %	99.9	100.0
GOF (F^2)	1.155	1.028
reflections with $I>2\sigma(I)$	1771	1140
$R_1(F)$ ($I>2\sigma(I)$)[a]	0.0426	0.0359
$wR_2(F^2)$ (all data)[b]	0.1125	0.0778
Largest diff. peak/hole, *e*·Å^{-3}	0.337 / -0.344	0.283 / -0.263

[a] $R_1 = \sum|F_o - |F_c||/\sum(F_o)$; [b] $wR_2 = (\sum[w(F_o^2 - F_c^2)^2]/\sum[w(F_o^2)^2]^{1/2}$

Crystal Structure of 5-(4-Azidofurazan-3-yl)-[1,2,3]triazolo[4,5-c][1,2,5]-oxadiazol-5-ium-4-ide (11)

An analysis of intermolecular contacts has revealed that all shortened contacts correspond to the $n\ldots\pi^*$ type of interactions. It can be explained by the electron deficient properties of heterocycles in compound **11**, and this observation is in agreement with our recent results on the analysis of furazan macrocycles in which prevalence of $n\ldots\pi^*$ over $\pi\ldots\pi^*$ type of interactions has been observed.[38e]

As we have done recently,[27g, 38e] in the present study both visual analysis that is based on consideration of the close intermolecular contacts, and energetic analysis based on pair intermolecular interaction energies were applied. For the latter approach, we used energies of pair intermolecular interactions obtained from the M052X/aug-cc-pvdz calculation[52] of dimers of the central molecule M0 with its closets surroundings (14 molecules, see Table S2 and Figure S4). Geometries of dimers were taken from the X-ray data; no additional optimization was carried out. We have recently shown that such way of an estimation of intermolecular interaction energy is in semiquantitative agreement with the method based on topological analysis of the electron density.[38e]

According to the visual analysis, the strongest interactions are formed for M0…G, H, K, L, M, N molecular pairs which are characterized by the presence of several shortened contacts for each pair. In part, it is in agreement with the results based on the energetic criteria. The M0…G, H, M, N interactions are the most energetically preferable, however the energy of M0…G, H pairs is nearly 2 times higher than that for M0…M, N pairs that is not evident from the visual analysis. At the same time, the energy of M0…K, L pairs is nearly equal to that of M0…E, F, I, J while for the latter pairs, no shortened contacts are observed.

The origin of the observed discrepancy is in the fact that the visual analysis is based on a consideration of the close contacts only, and does not take into account weak van-der-Waals interactions while the energy of molecular pairs include all interactions. Therefore energetic approach appears to be more general and straightforward, but it requires additional calculation. At the same time, visual analysis shows what intermolecular interactions are responsible for the predominant contribution to the total energy, thereby providing complementary information to the energetic approach.

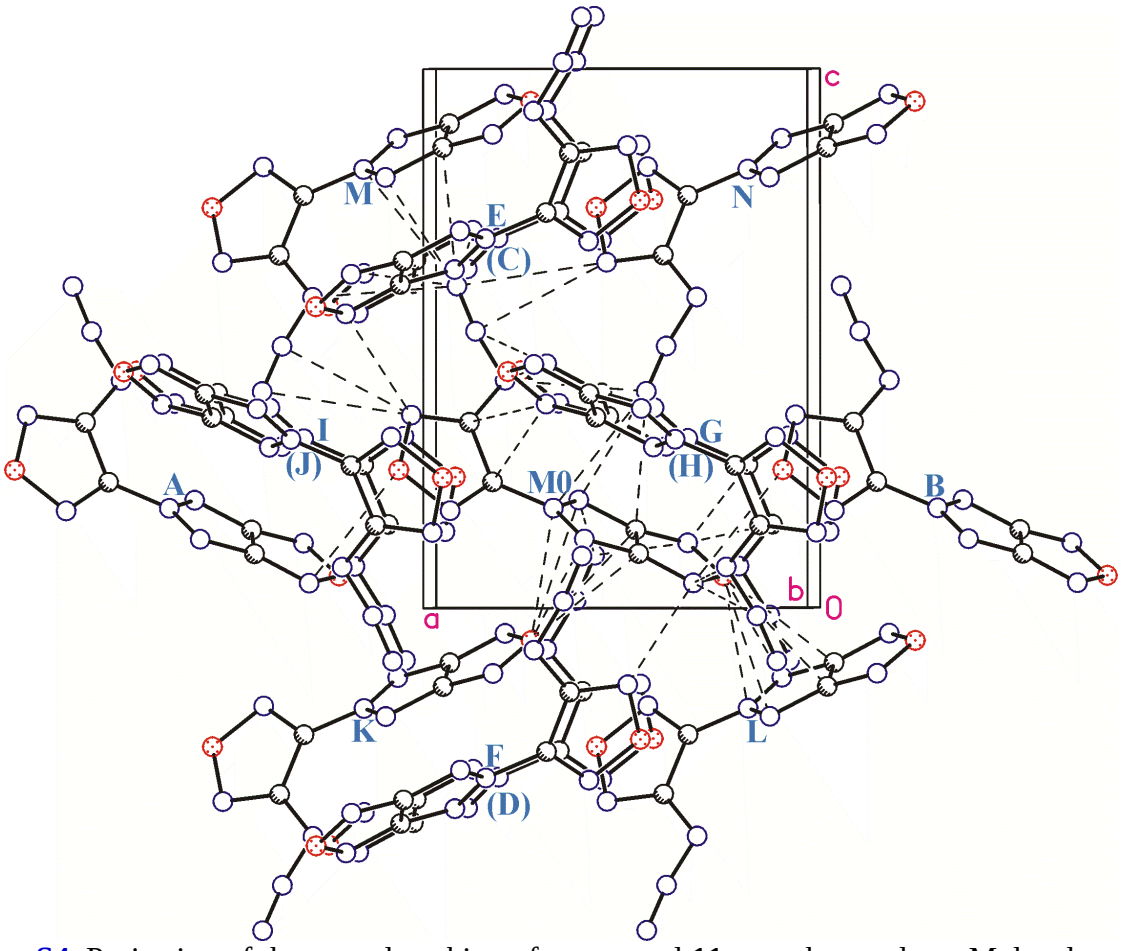

Figure S4. Projection of the crystal packing of compound **11** onto the *ac* plane. Molecules of the closest surroundings of the central molecule M0 are denoted by capital letters and correspond to those in Table S2. Letters in parentheses correspond to molecules located below the plane of the figure (obtained by a translation along the axis *b*).

Table S2. Close contacts (Å) and intermolecular interaction energies (kcal/mol) for the interaction of the central molecule M0 with its closest surroundings as obtained from quantum chemical (M052X/aug-cc-pvdz) calculation for structure **11**.

Neighbour of M0	Close contact	Distance	Symmetry code	Energy
A	O1…N7	3.115	1+x,y,z	-1.0
B	N7…O1	3.115	-1+x,y,z	-1.0
C	N10…N4 N10…N6	3.196 3.177	1.5-x,1-y,1/2+z	-0.3
D	N4…N10 N6…N10	3.196 3.177	1.5-x,1-y,-1/2+z	-0.3
E	N2…N7	3.155	1.5-x,2-y,1/2+z	-1.9
F	N7…N2	3.155	1.5-x,2-y,-1/2+z	-1.9
G	N7…N8 N7…N9 C1…N6 C2…N6	3.014 2.974 3.022 3.220	1-x,1/2+y,1/2-z	-5.6
H	N6…C1 N6…C2 N8…N7 N9…N7	3.022 3.220 3.014 2.974	1-x,-1/2+y,1/2-z	-5.6
I	No close contact		2-x,1/2+y,1/2-z	-2.1
J	No close contact		2-x,-1/2+y,1/2-z	-2.1
K	N3…O2 N4…O2 N5…O2 C3…O2 C4…O2	2.960 3.143 3.042 3.212 3.141	1/2+x,1.5-y,-z	-1.9
L	O2…N3 O2…N4 O2…N5 O2…C3 O2…C4	2.960 3.143 3.042 3.212 3.141	-1/2+x,1.5-y,-z	-1.9
M	N10…N3 N10…N4 N10…N8 N10…C3 N2…N9 N2…N10	3.145 3.020 3.202 3.148 3.165 3.197	1/2+x,1.5-y,1-z	-3.0
N	N3…N10 N4…N10 N8…N10 C3…N10 N9…N2 N10…N2	3.145 3.020 3.202 3.148 3.165 3.197	-1/2+x,1.5-y,1-z	-3.0

Based on energetic analysis, one can separate chains along *b* crystallographic axis (Figure S5) formed by M0…G, H interactions as being the strongest ones; the predominant contribution to this energy arises from the $n\ldots\pi^*$ interaction of the N7 atom with the π-system of the azido group, and the N6 atom with the π-system of the furazan ring. The other weaker interactions connect chains into the 3-D structure.

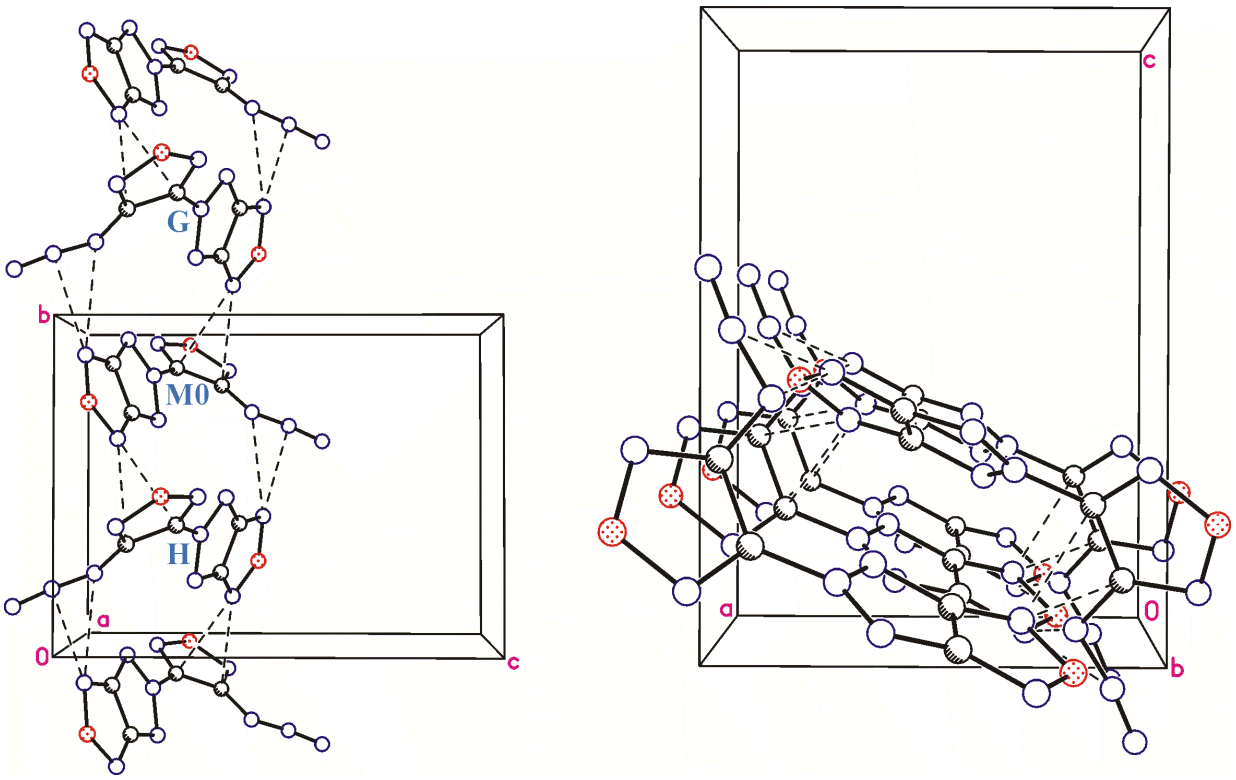

Figure S5. View of the chain along *b* crystallographic axis formed by M0…G and M0…H interactions. Left – projection onto *bc* plane. Right – projection onto *ac* plane

It can also be seen that no sufficiently close contacts are observed in the crystal structure of compound **11** in spite of its high density. Except for the few ones, all shortened contacts (Table 2S) appear to be only slightly shorter than sum of van-der-Waals radii of corresponding atoms.[53] We believe that high density of compound **11** is provided by easiness of molecules to come closer to each other due to an absence of the strong interaction that can restrict molecular freedom of movement.

References

48. L. Garcia-Cruz, J. Iniesta, T. Thiemann, and V. Montiel. *Electrochem. Commun.*, 2012, **22**, 200-202.

49. H. Tian, M. Jia, M. Zhang, and J. Hu. *Electrochimica Acta*, 2013, **96**, 285–290.

50. APEX2 and SAINT. Bruker AXS Inc., Madison, Wisconsin, USA, 2009.

51. G. M. Sheldrick, *Acta Crystallogr*. 2008, **A64**, 112.

52. M. J. Frisch, G. W. Trucks, H. B. Schlegel, G. E. Scuseria, M. A. Robb, J. R. Cheeseman, J. A., Jr. Montgomery, K. N. Kudin, J. C. Burant, J. M. Millam, S. S. Iyengar, J. Tomasi, V. Barone, B. Mennucci, M. Cossi, G. Scalmani, N. Rega, G. A. Petersson, H. Nakatsuji, M. Hada, M. Ehara, K. Toyota, R. Fukuda, J. Hasegawa, M. Ishida, T. Nakajima, Y. Honda, O. Kitao, H. Nakai, M. Klene, X. Li, J. E. Knox, H. P. Hratchian, J. B. Cross, V. Bakken, C. Adamo, J.

Jaramillo, R. Gomperts, R. E. Stratmann, O. Yazyev, A. J. Austin, R. Cammi, C. Pomelli, J. W. Ochterski, P. Y. Ayala, K. Morokuma, G. A. Voth, P. Salvador, J. J. Dannenberg, V. G. Zakrzewski, S. Dapprich, A. D. Daniels, M. C. Strain, O. Farkas, D. K. Malick, A. D. Rabuck, K. Raghavachari, J. B. Foresman, J. V. Ortiz, Q. Cui, A. G. Baboul, S. Clifford, J. Cioslowski, B. B. Stefanov, G. Liu, A. Liashenko, P. Piskorz, I. Komaromi, R. L. Martin, D. J. Fox, T. Keith, M. A. Al-Laham, C. Y. Peng, A. Nanayakkara, M. Challacombe, P. M. W. Gill, B. Johnson, W. Chen, M. W. Wong, C. Gonzalez, J. A. Pople, *Gaussian 03, ReVision E.01*; Gaussian, Inc.: Wallingford, CT, 2004.

53. R. S. Rowland and R.Taylor. *J. Phys. Chem.* 1996, **100**, 7384.

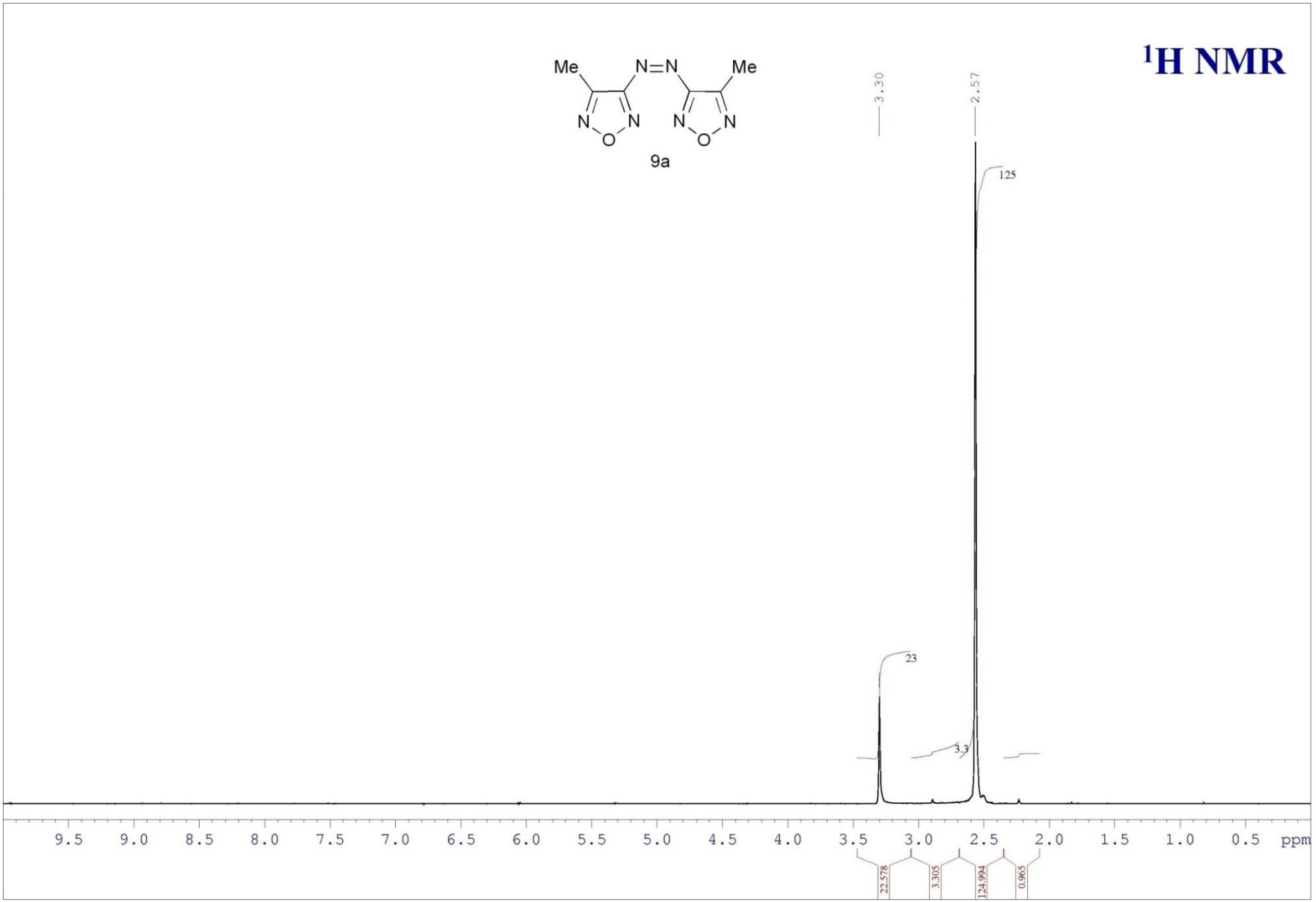

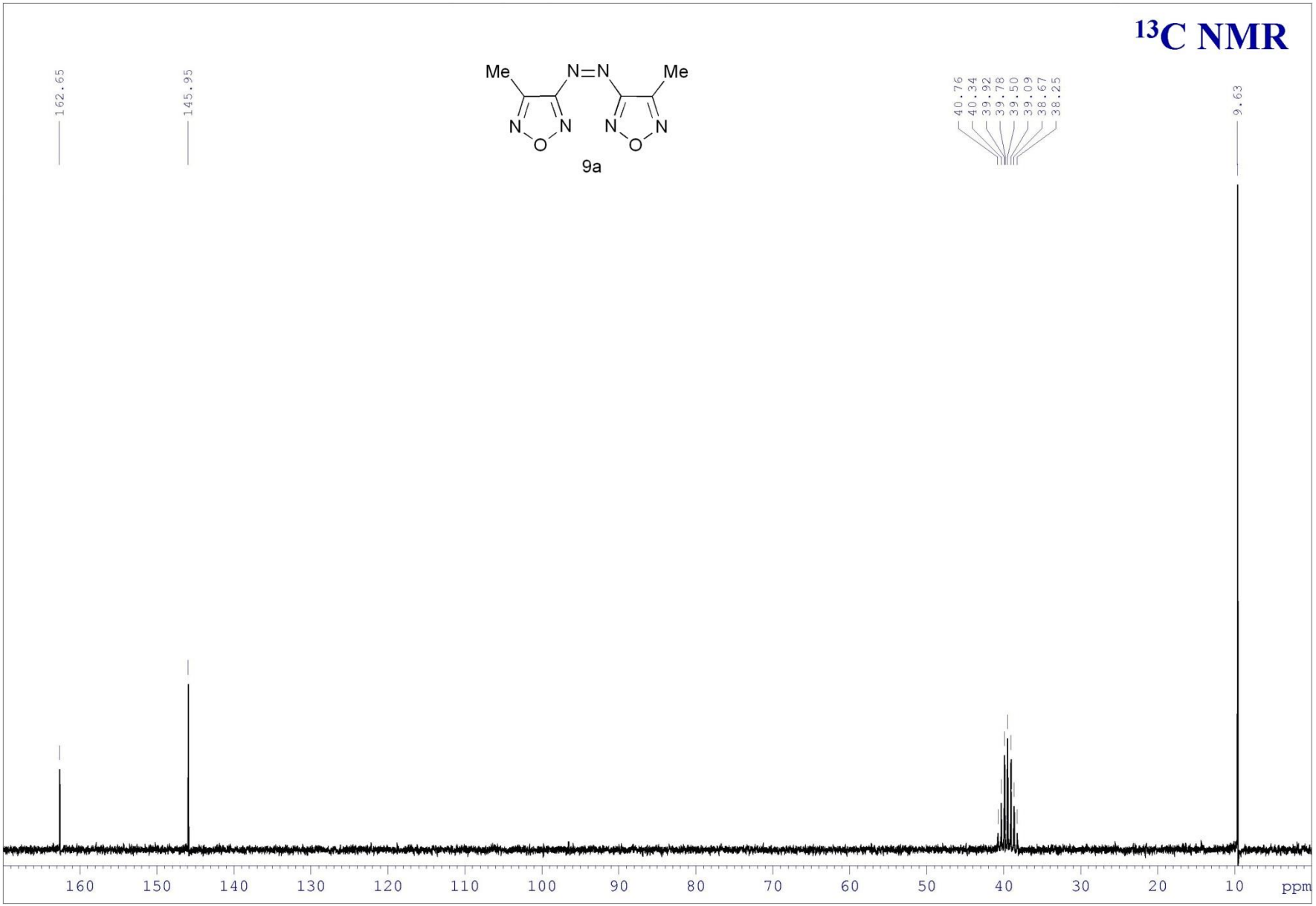

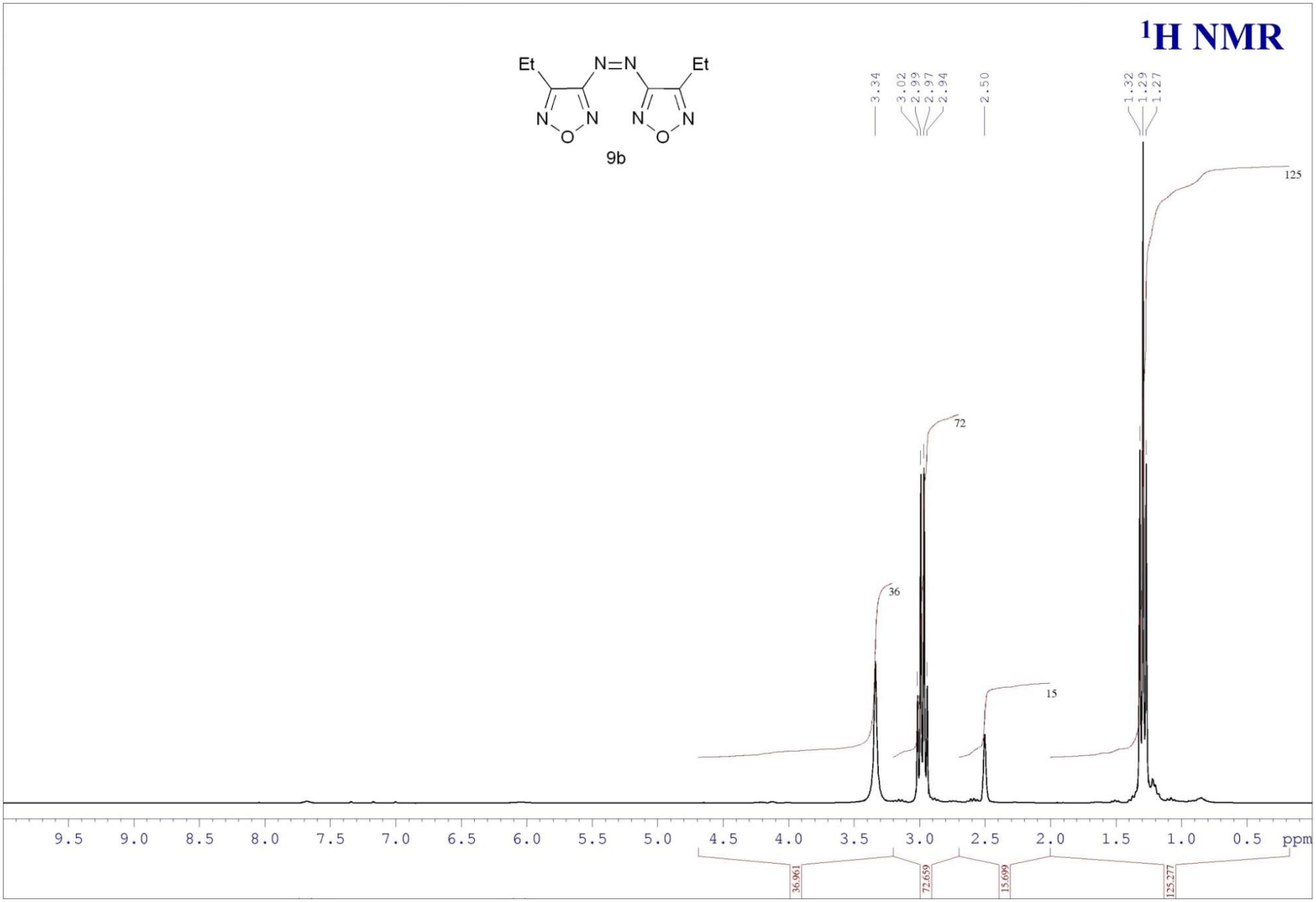

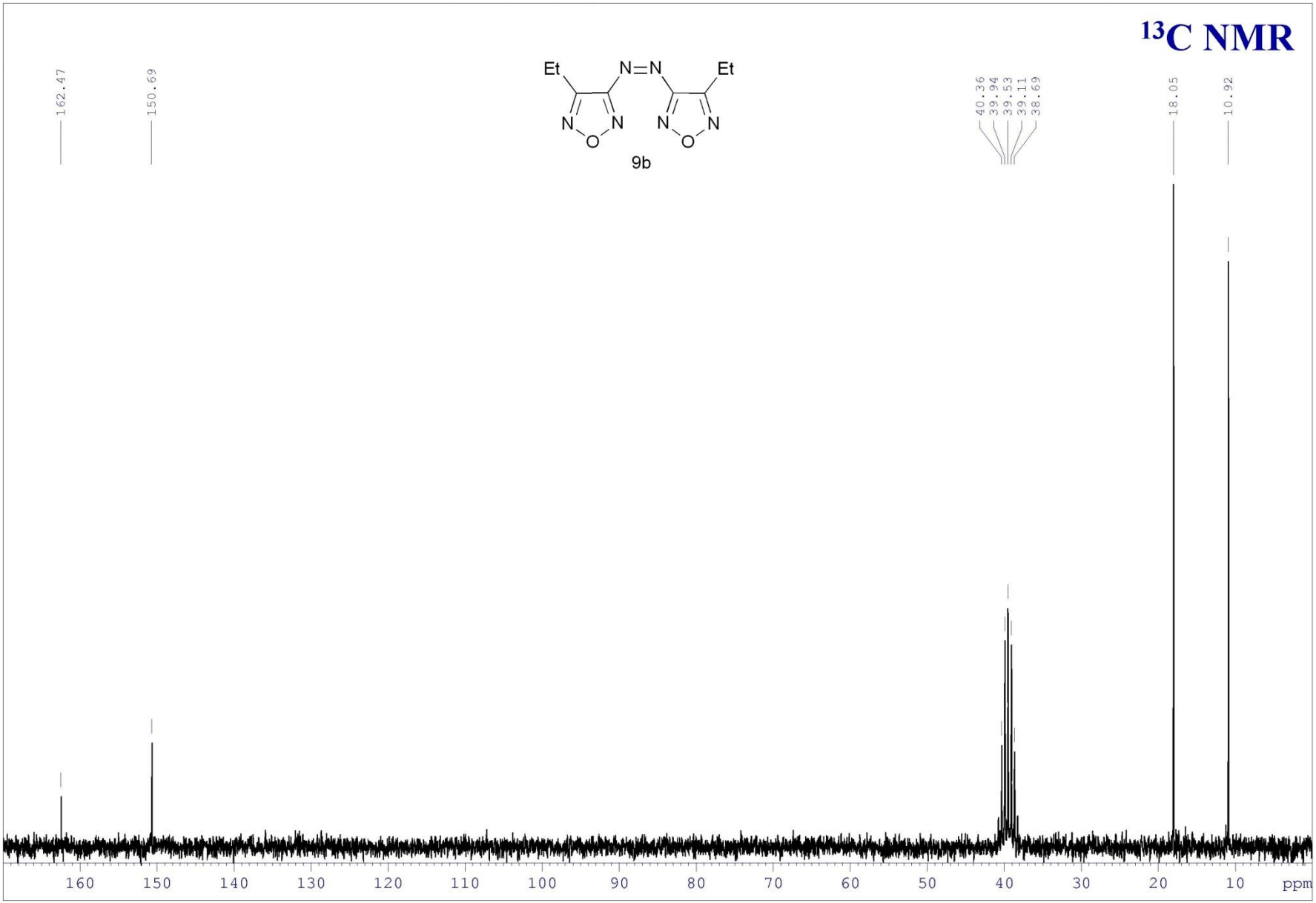

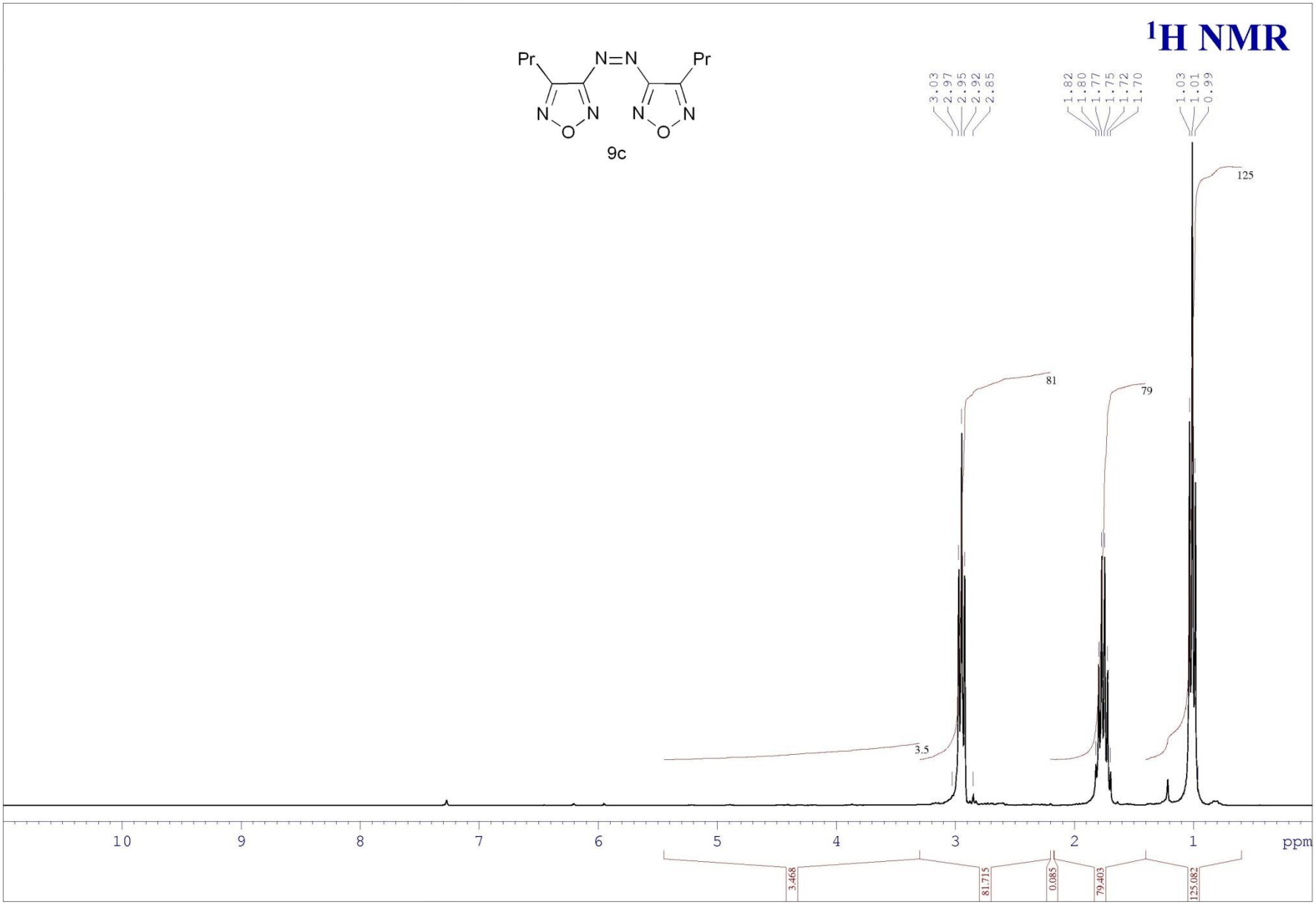

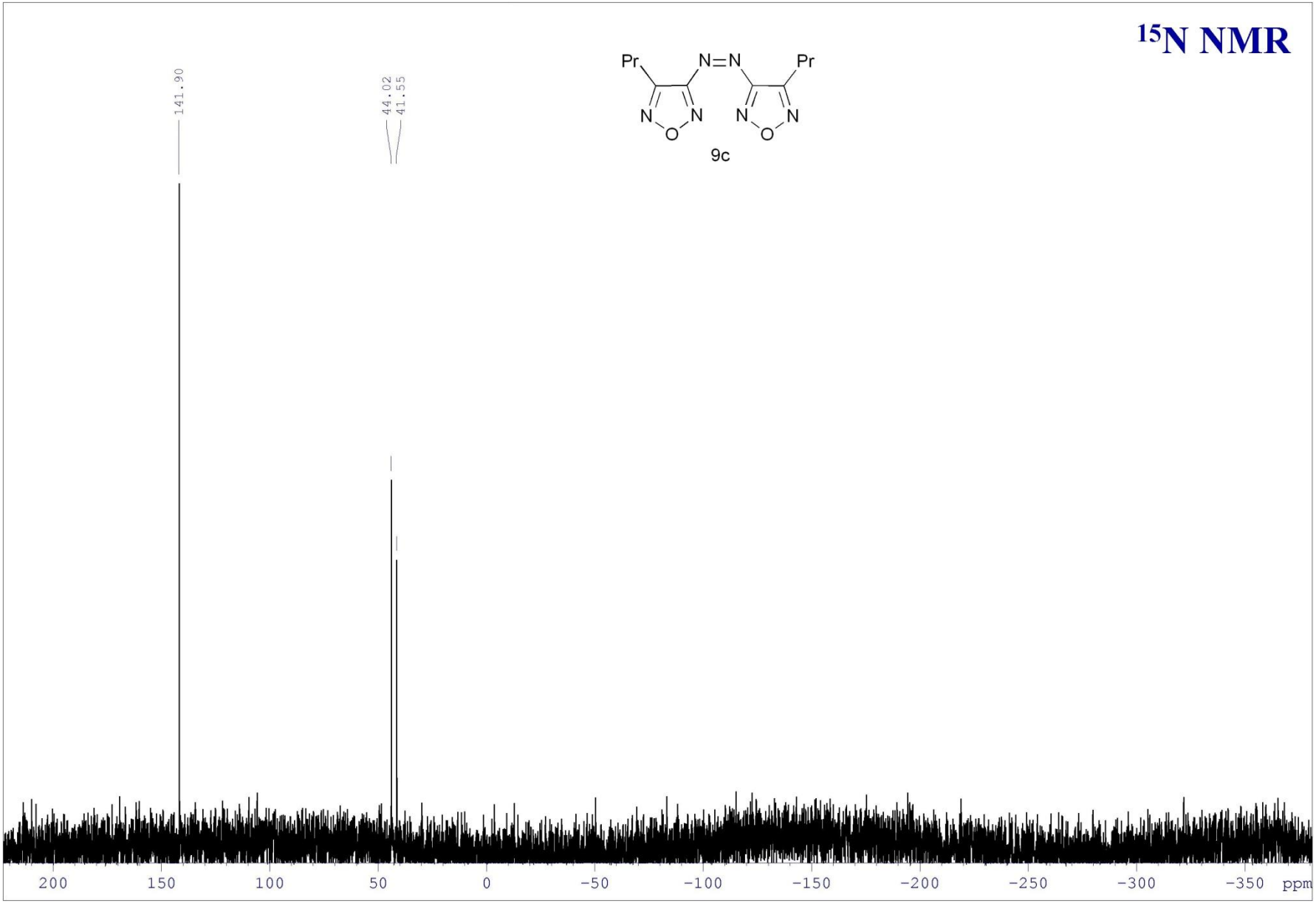

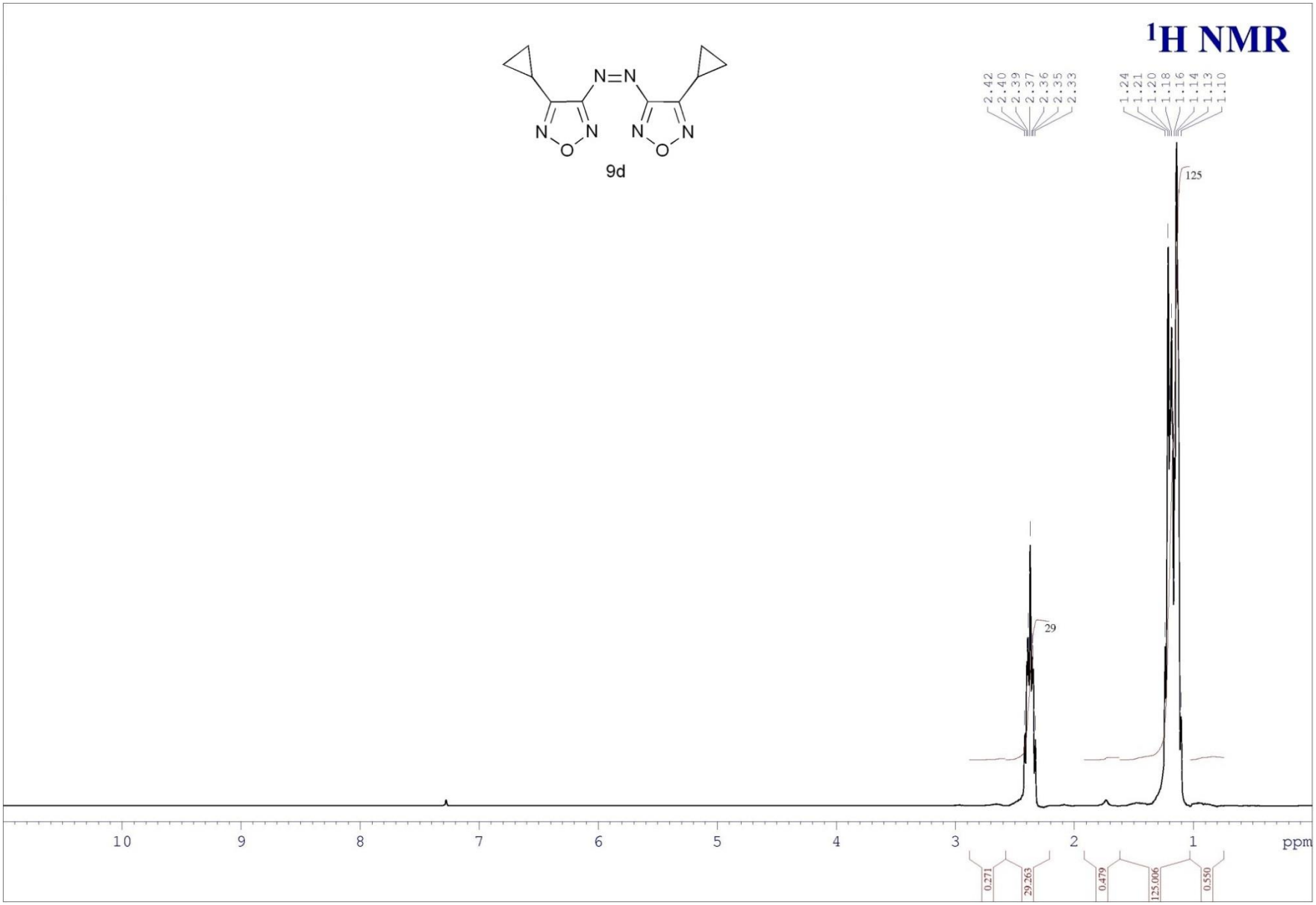

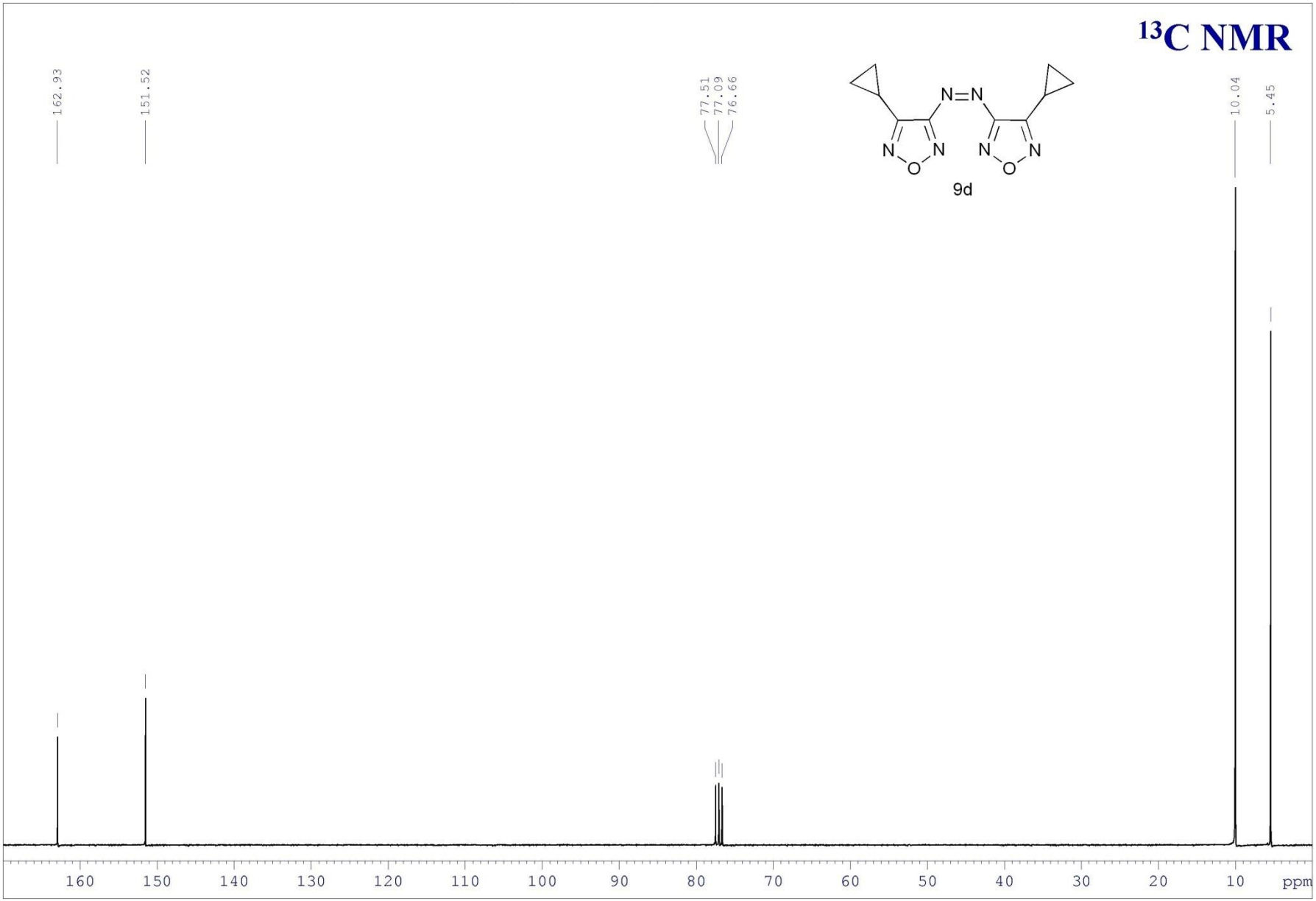

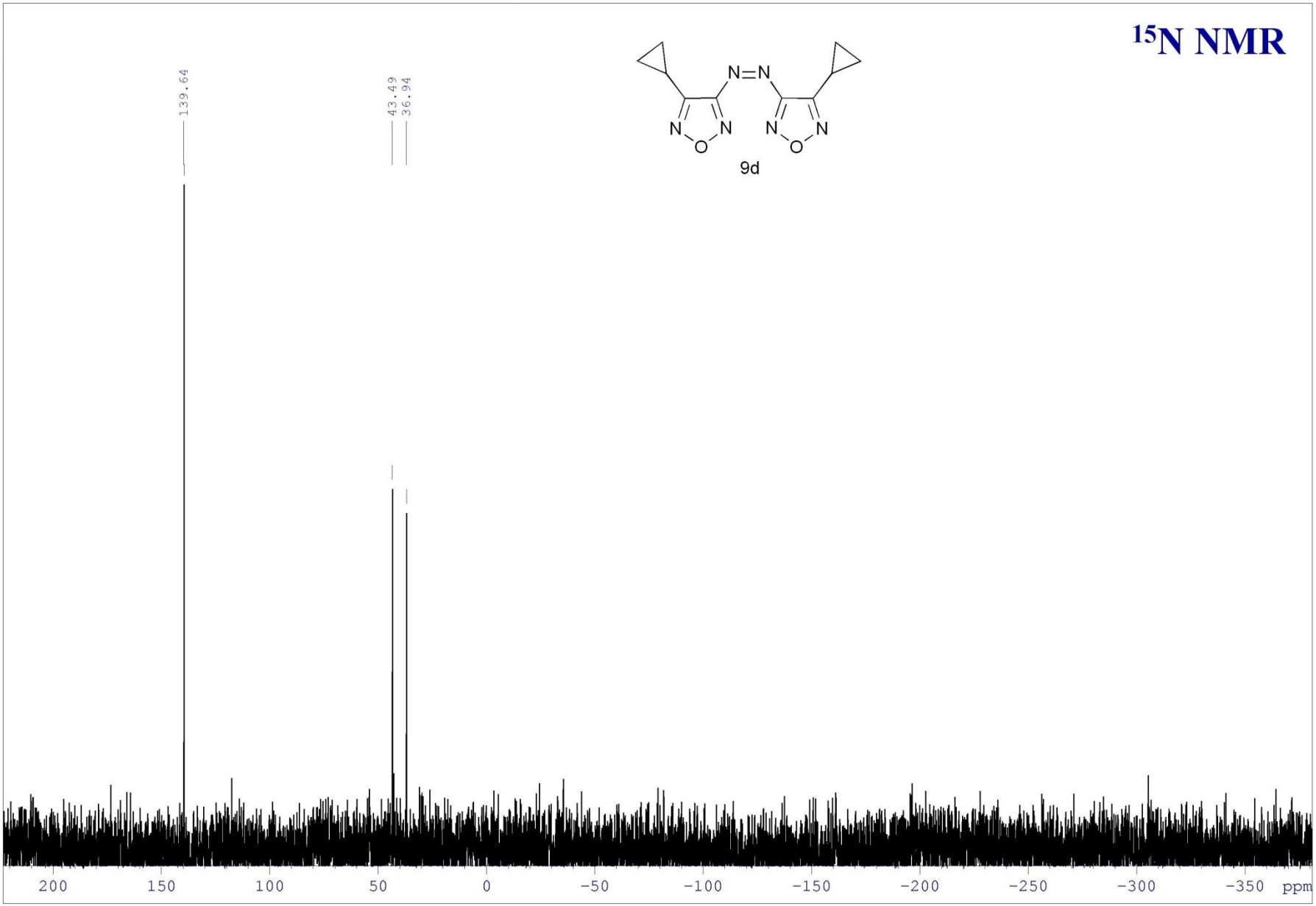

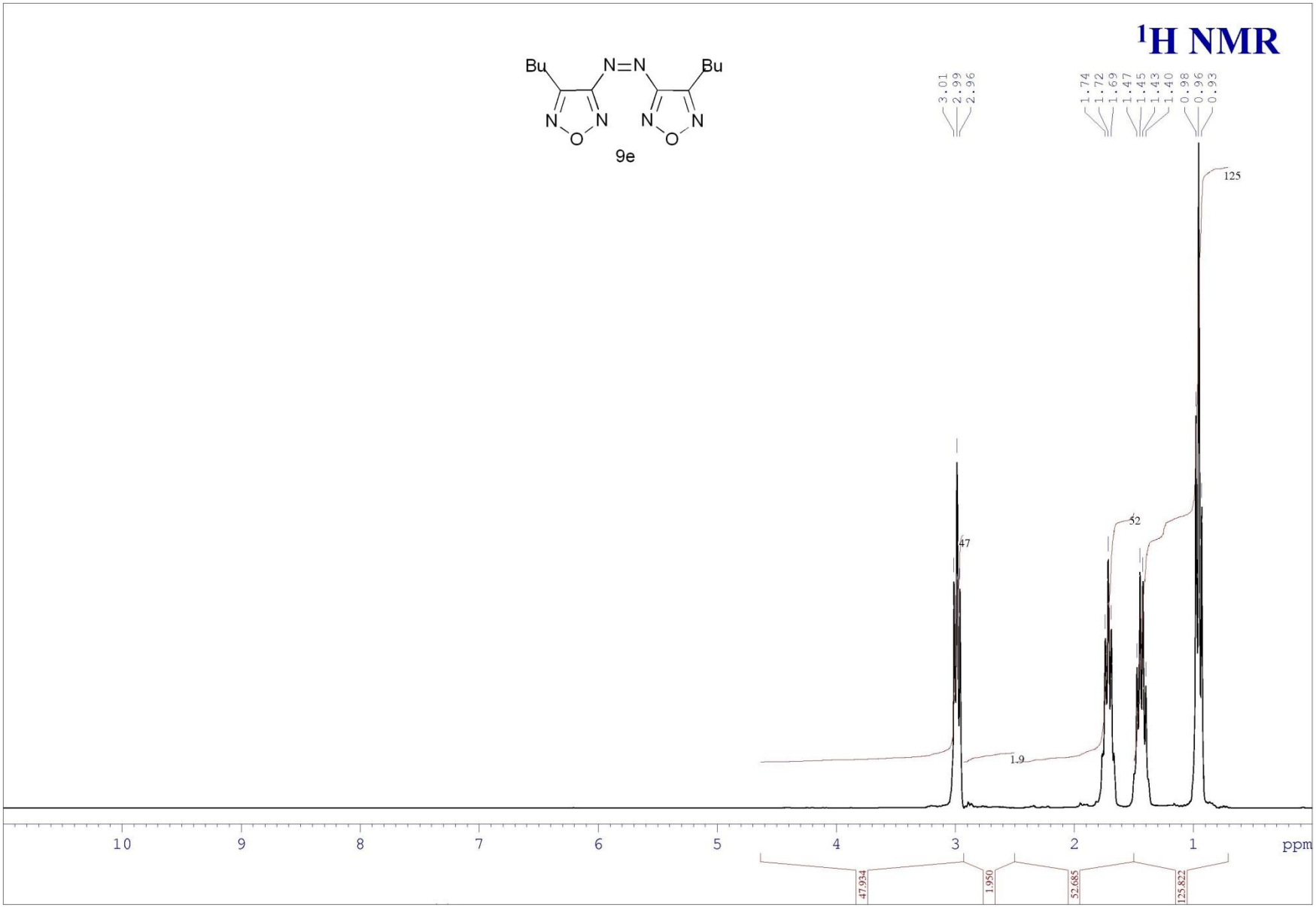

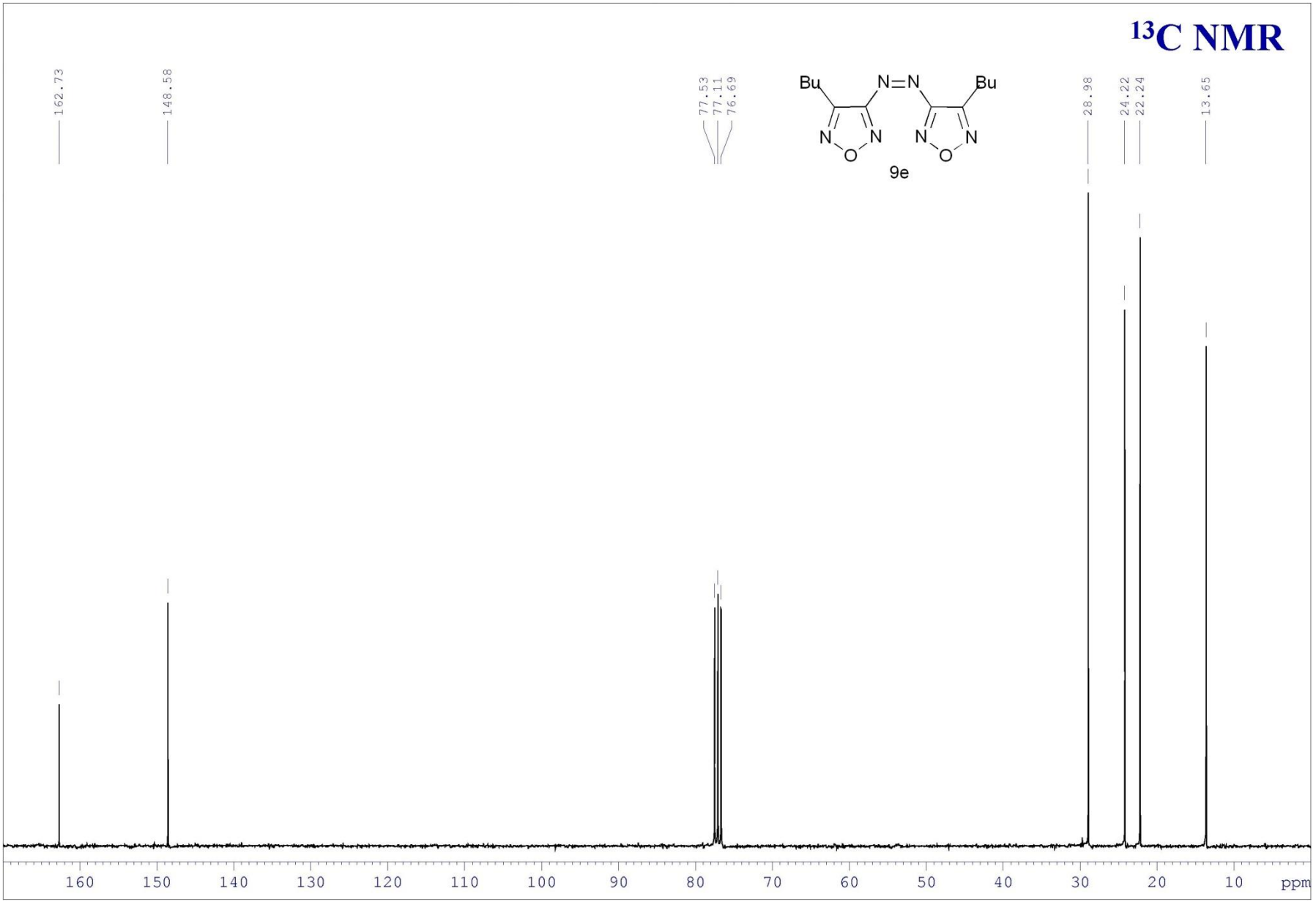

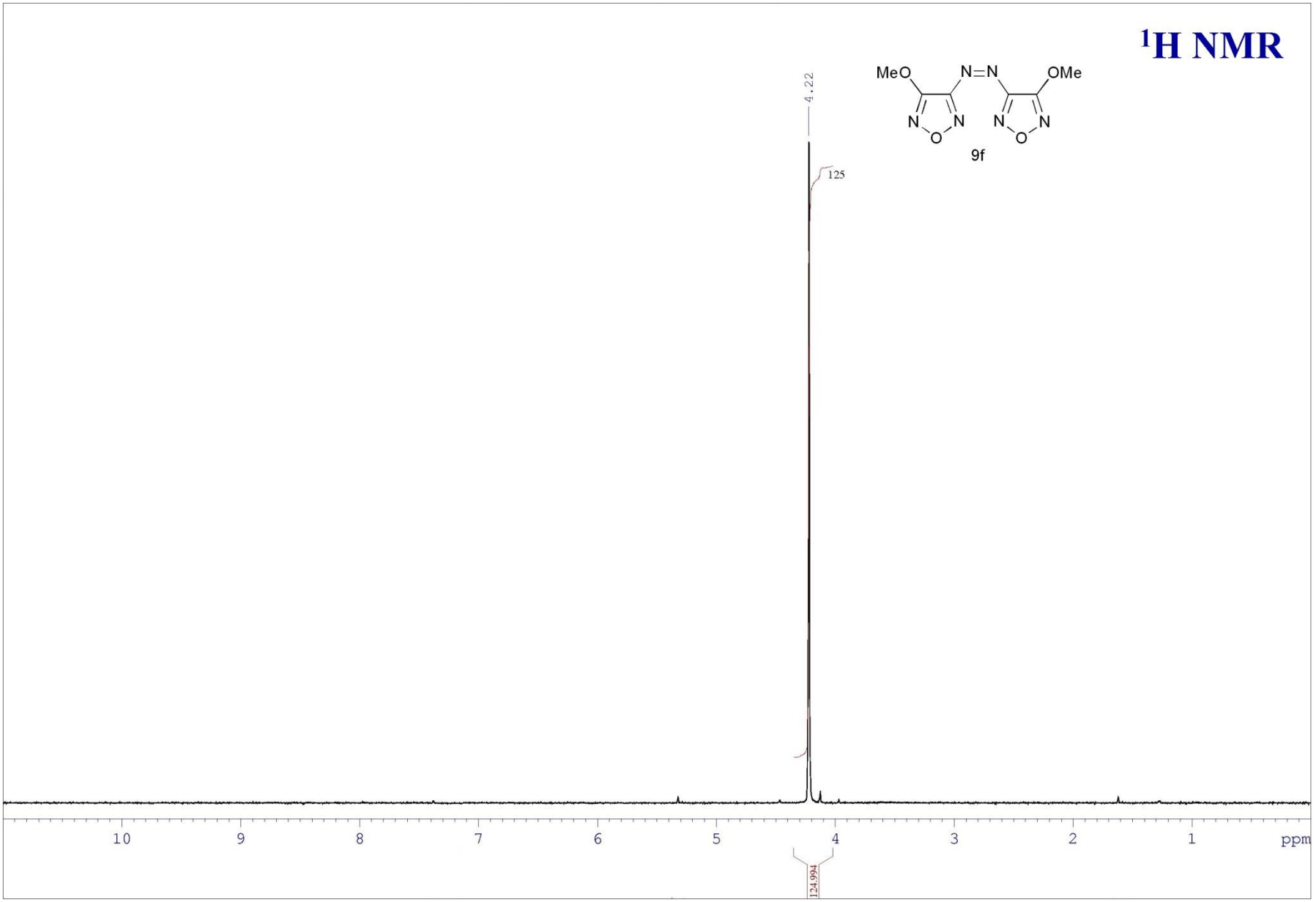

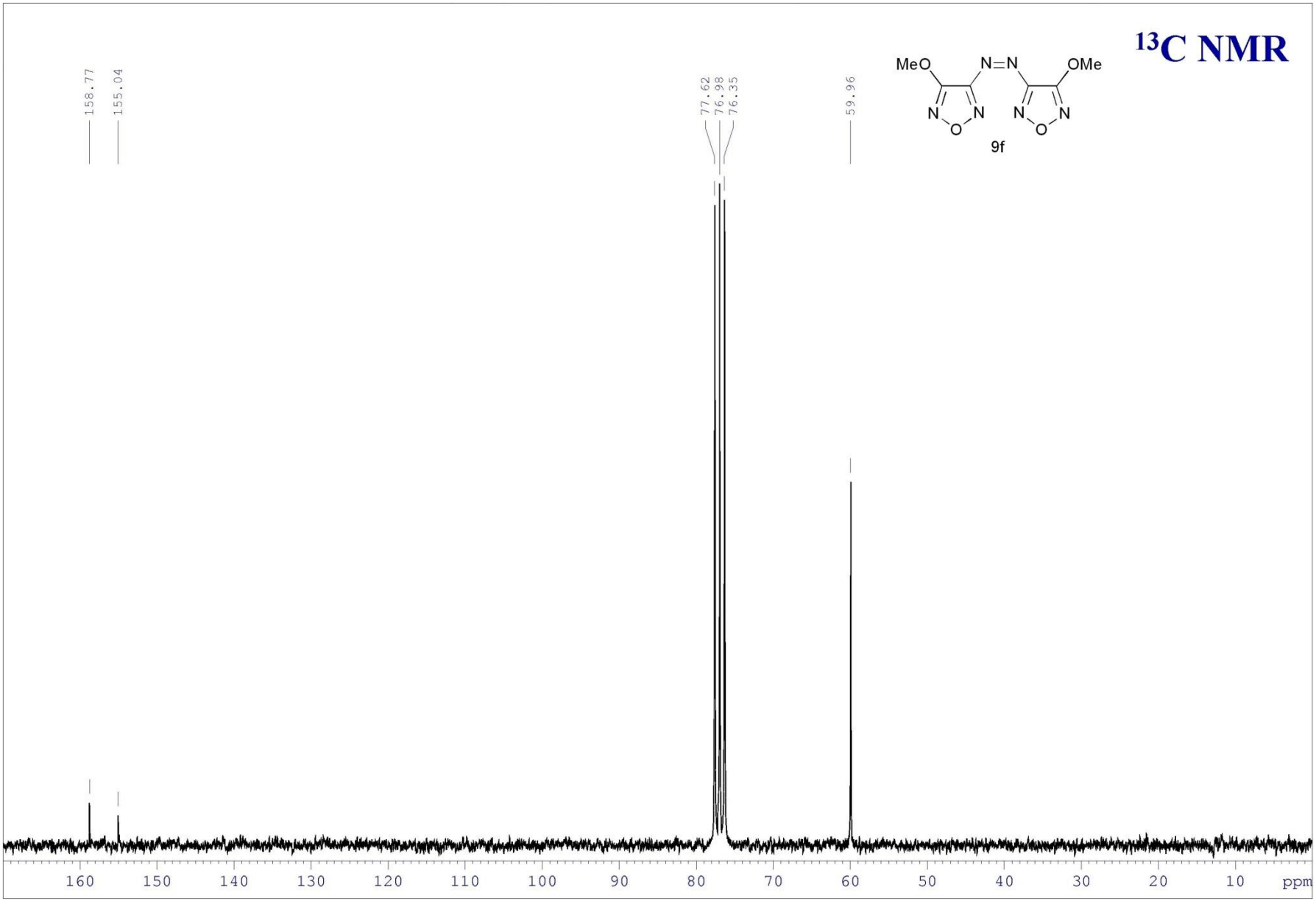

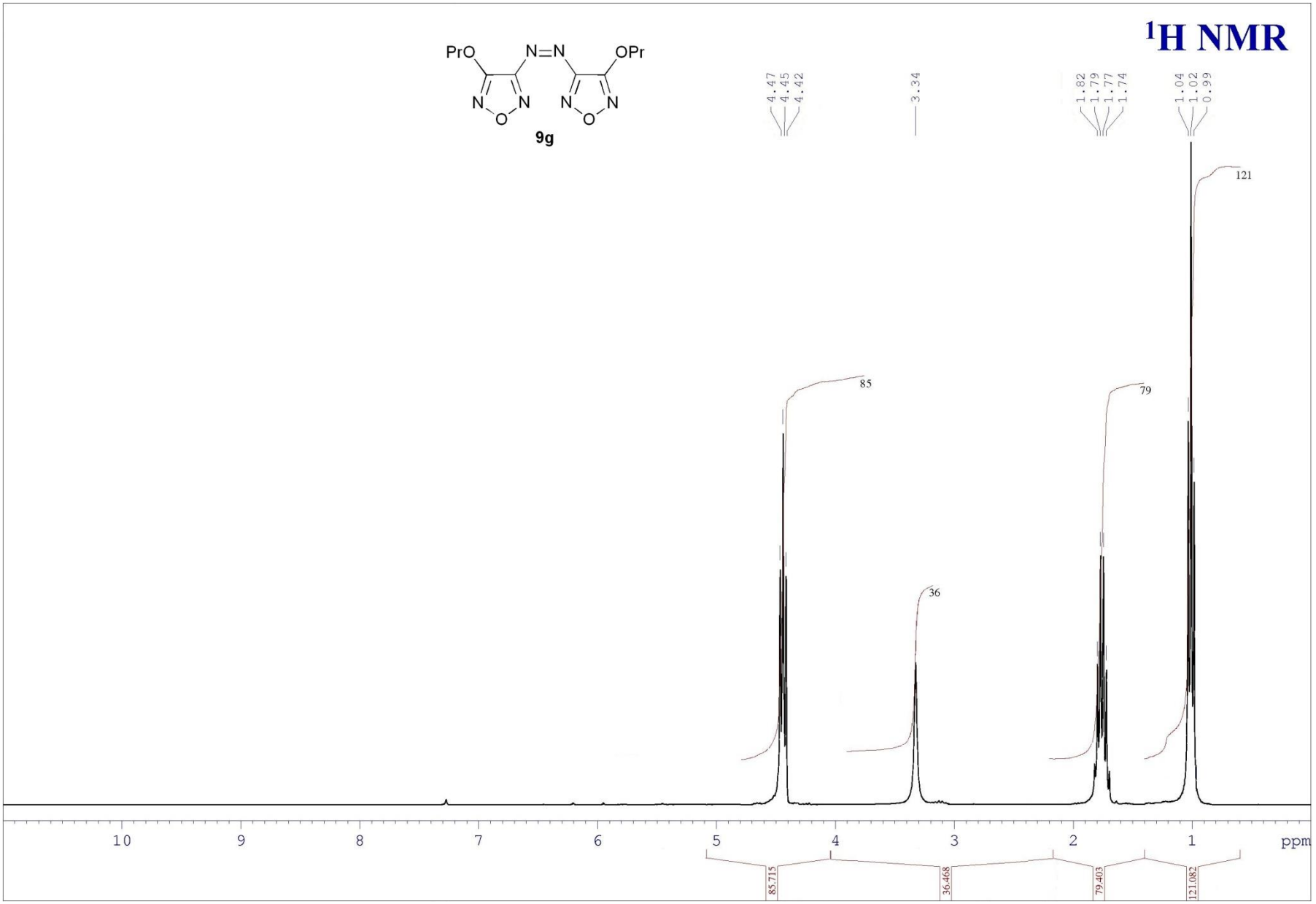

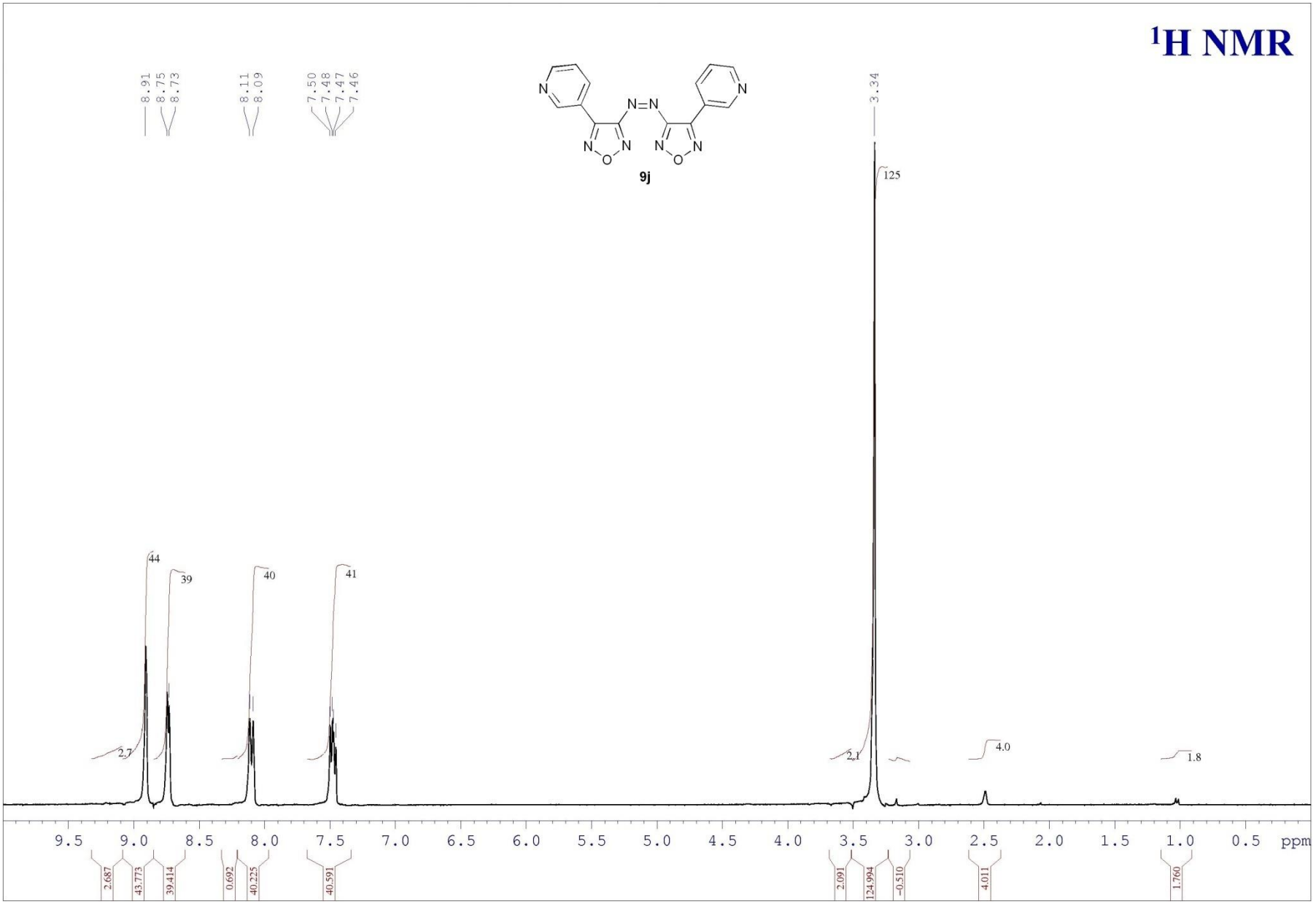

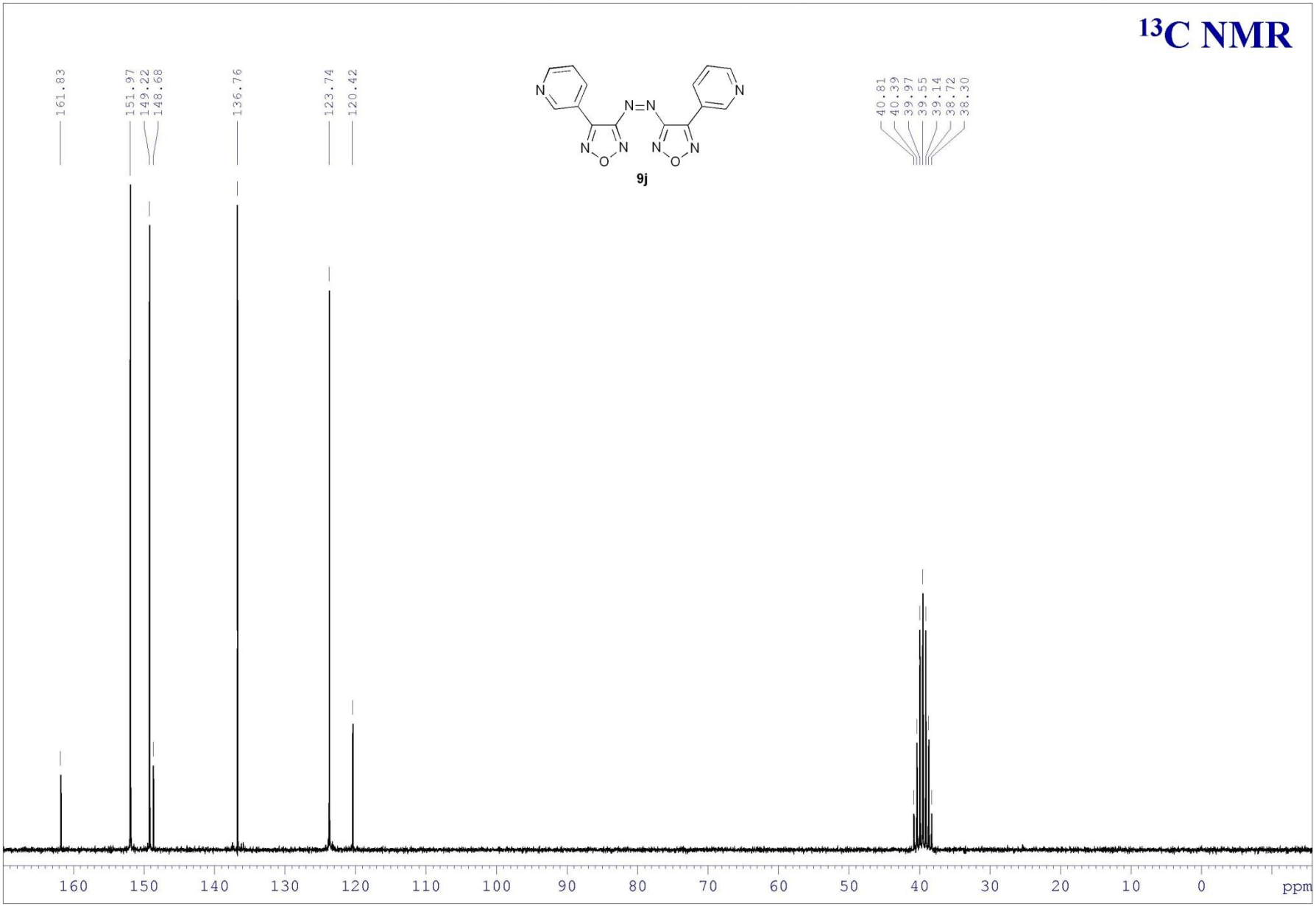

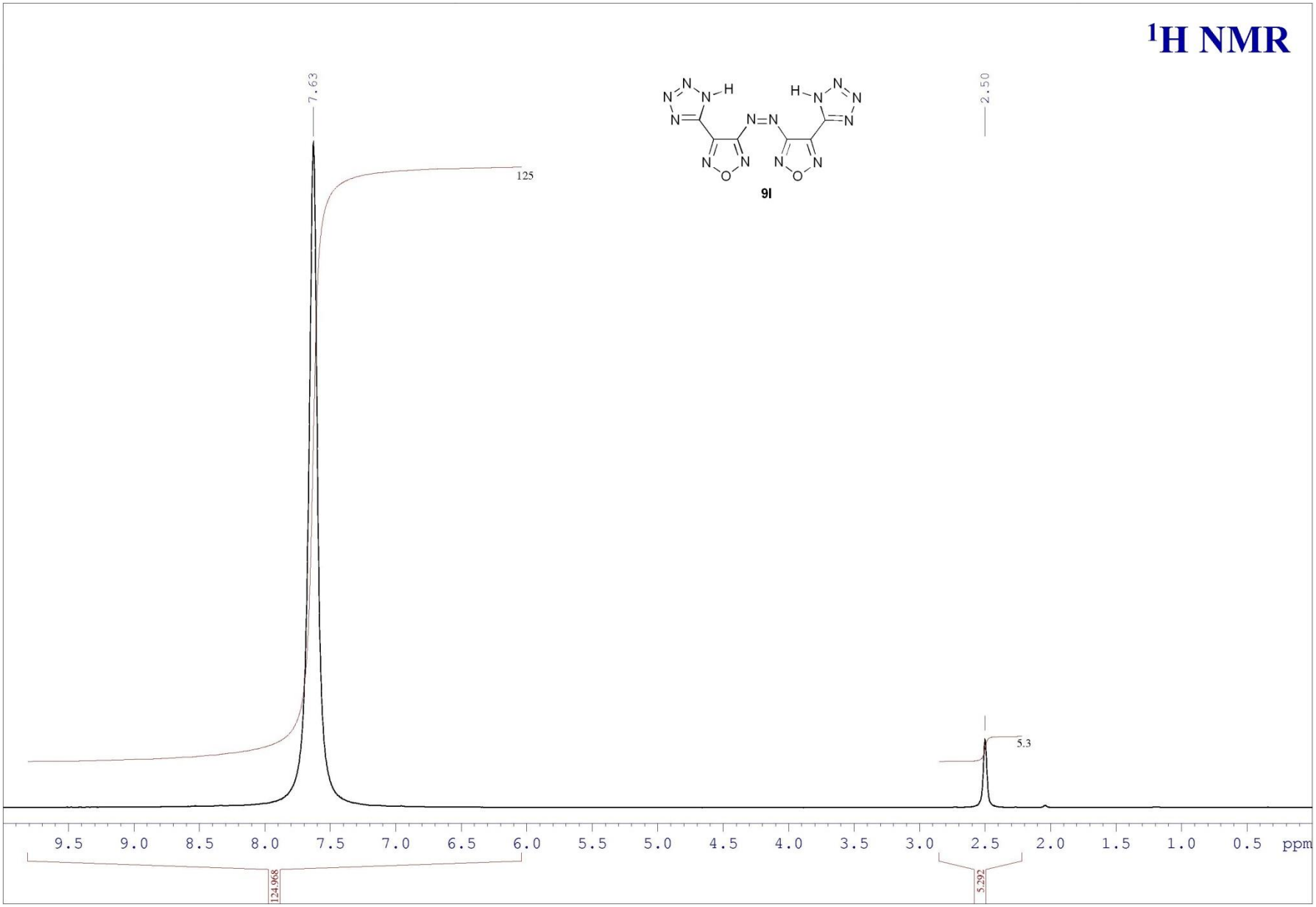

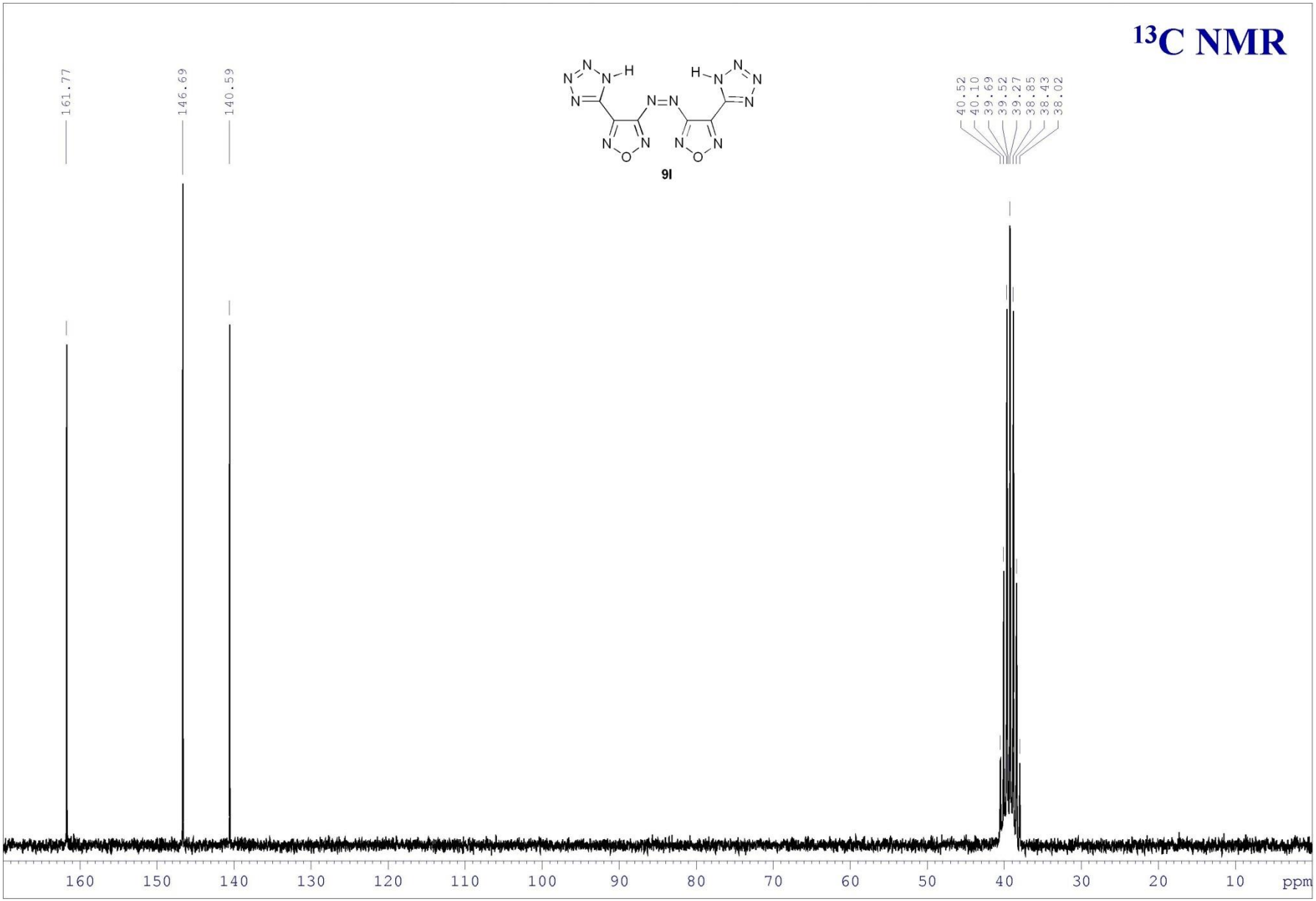

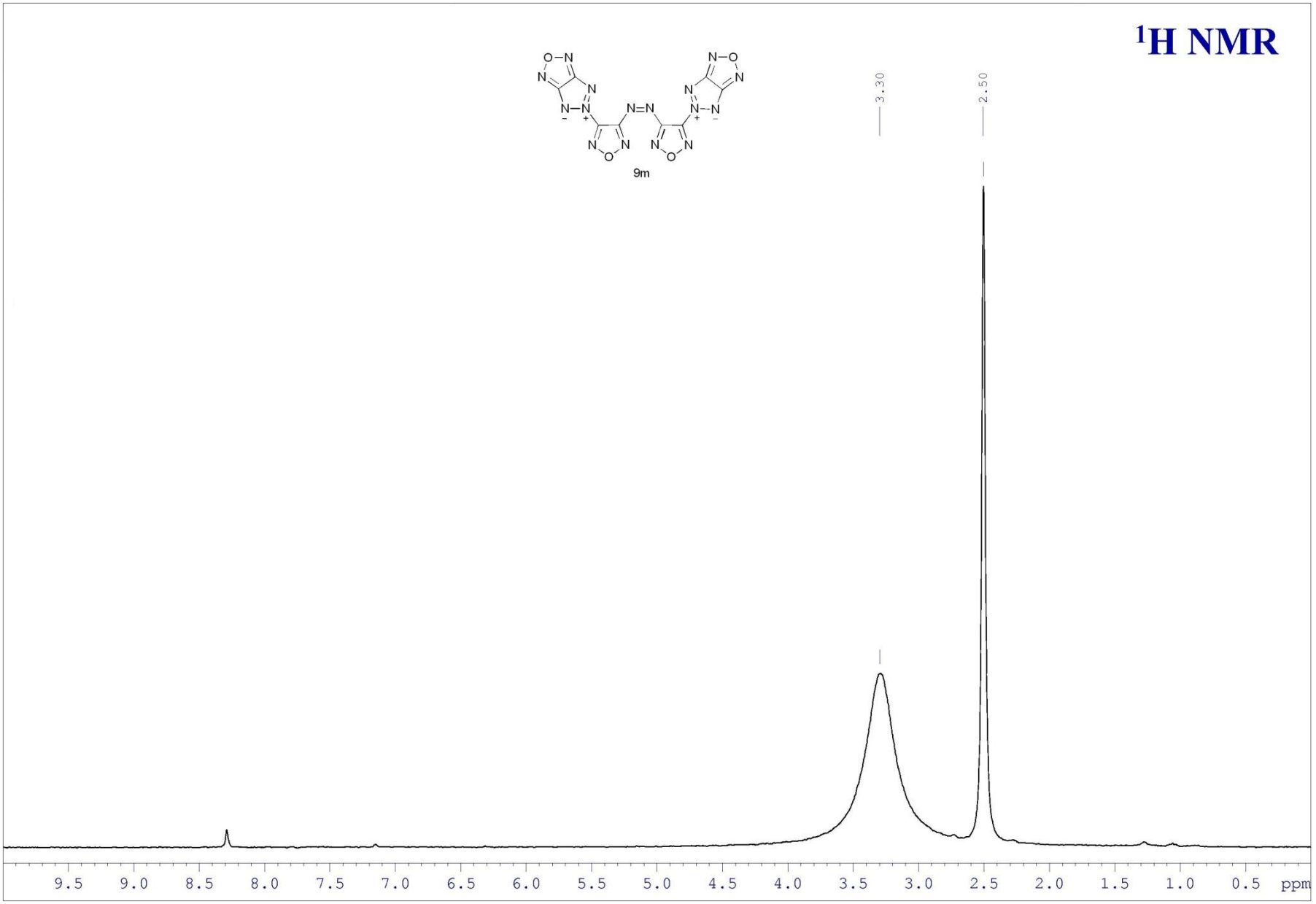

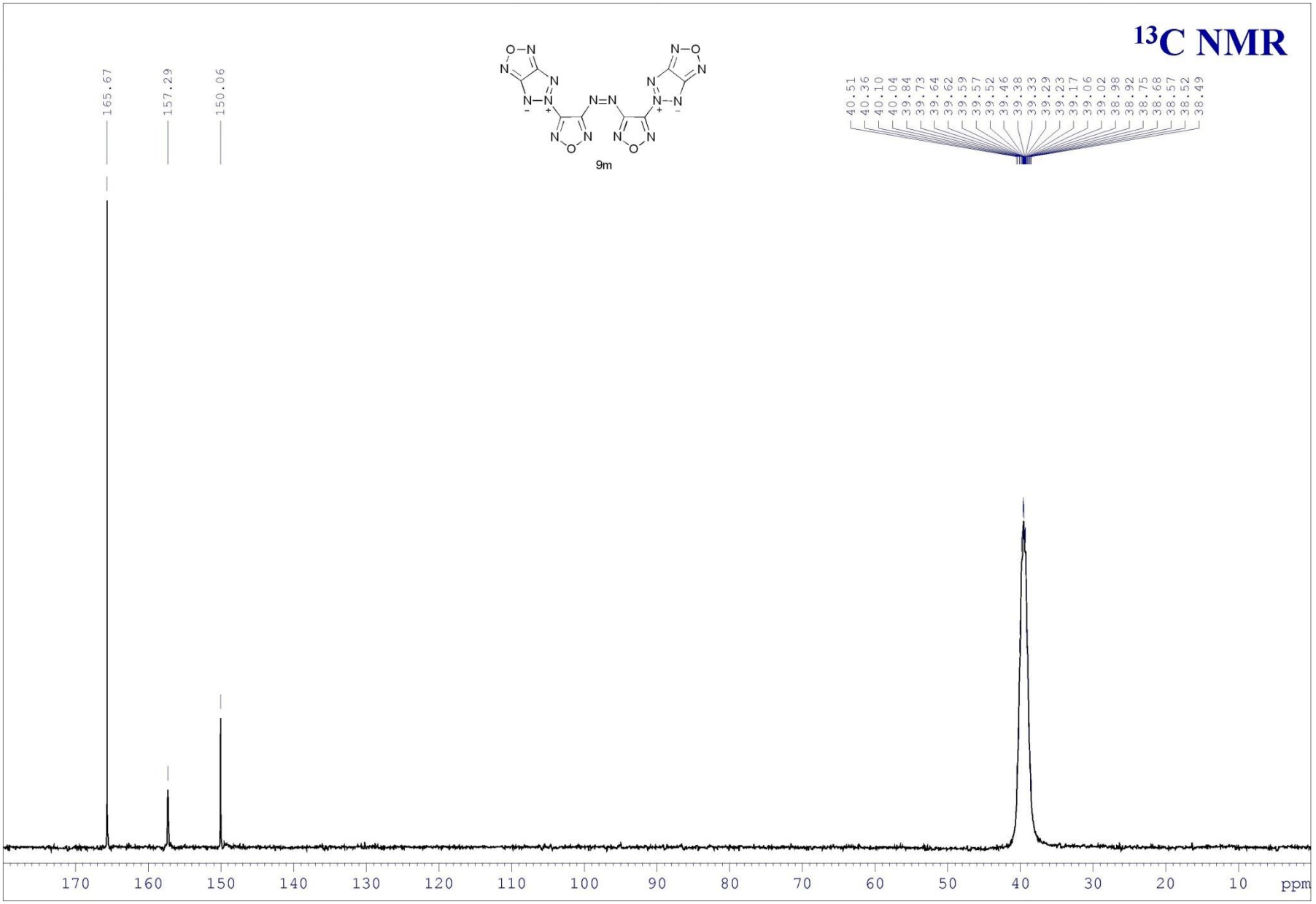

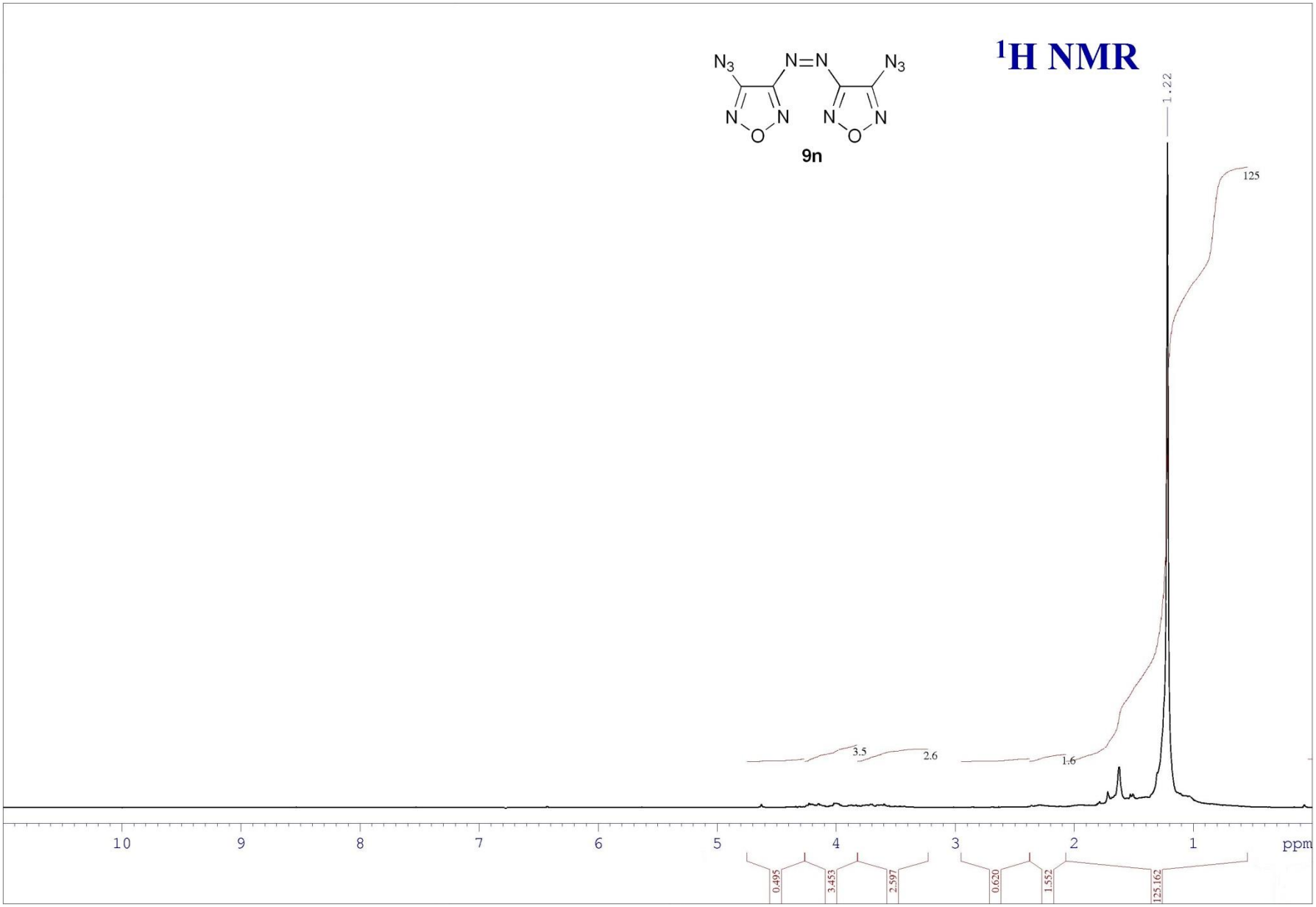

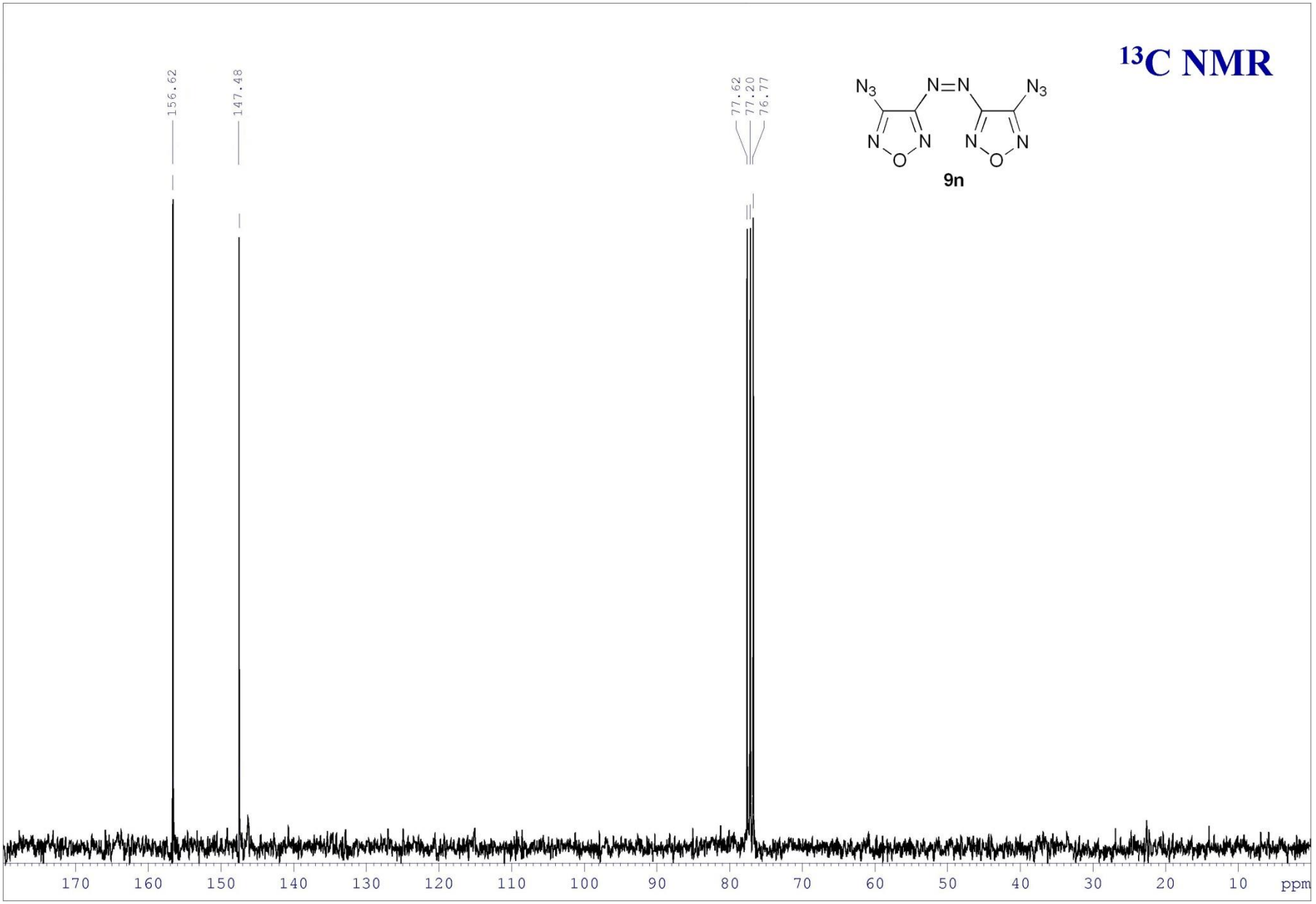

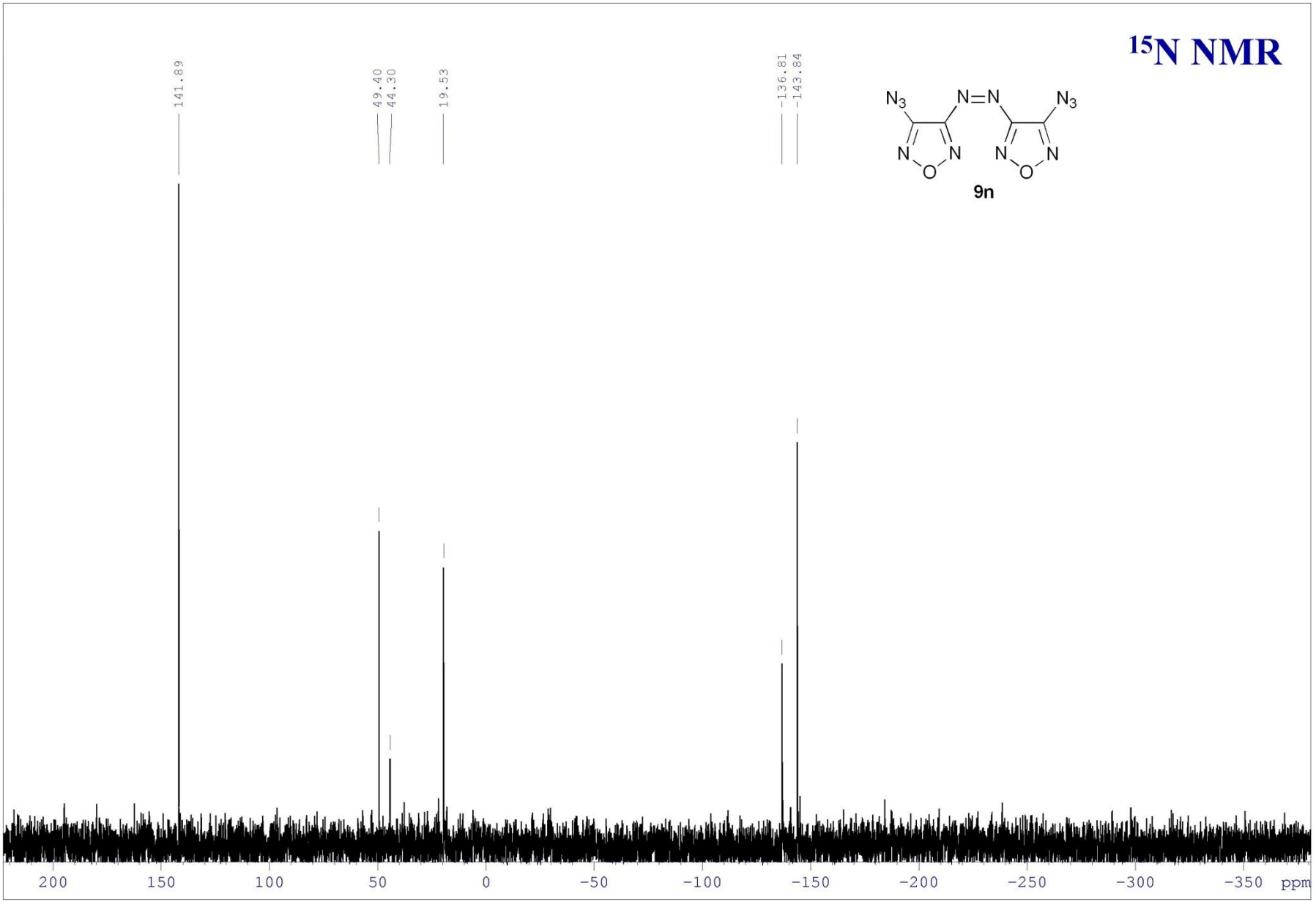

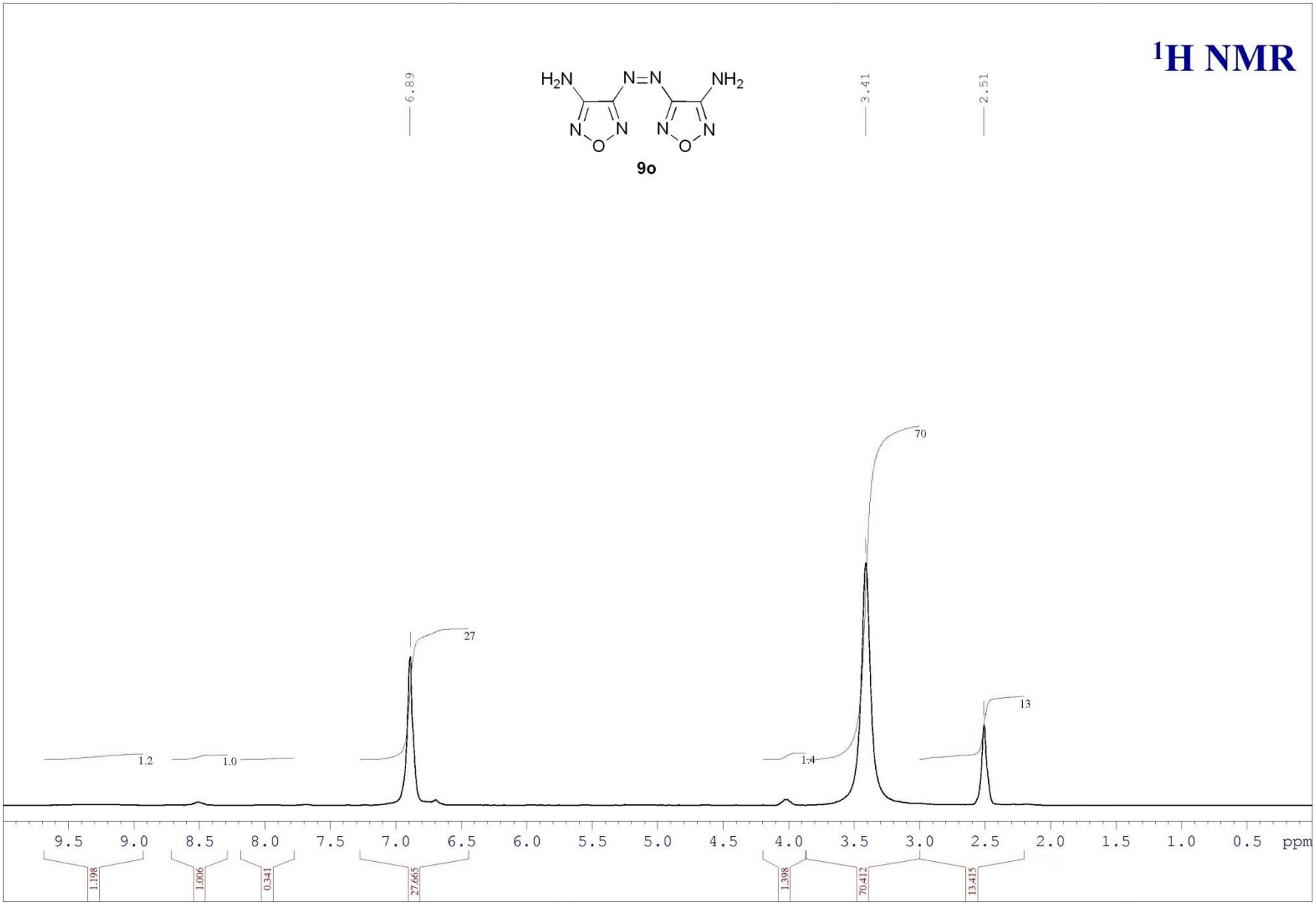

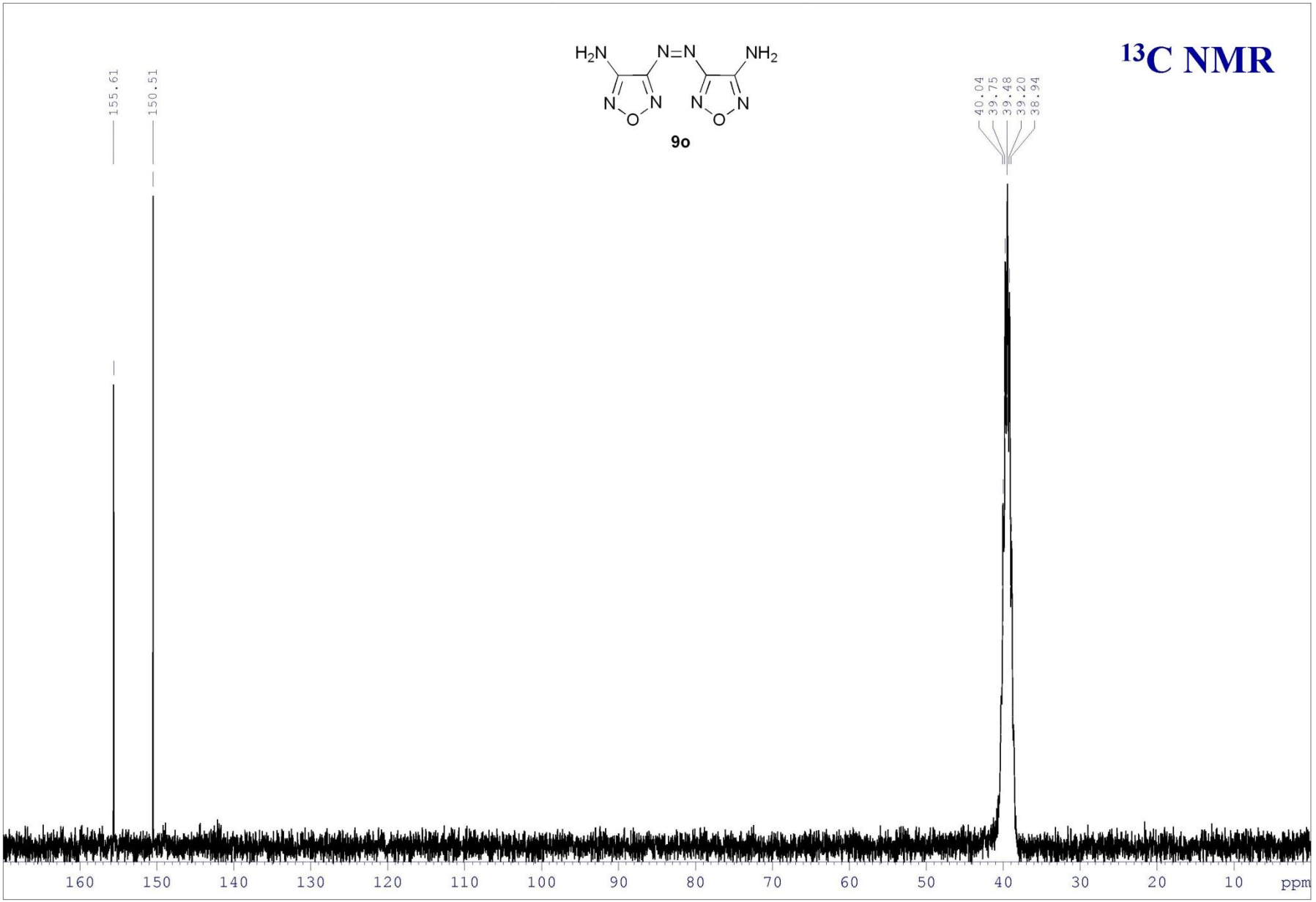

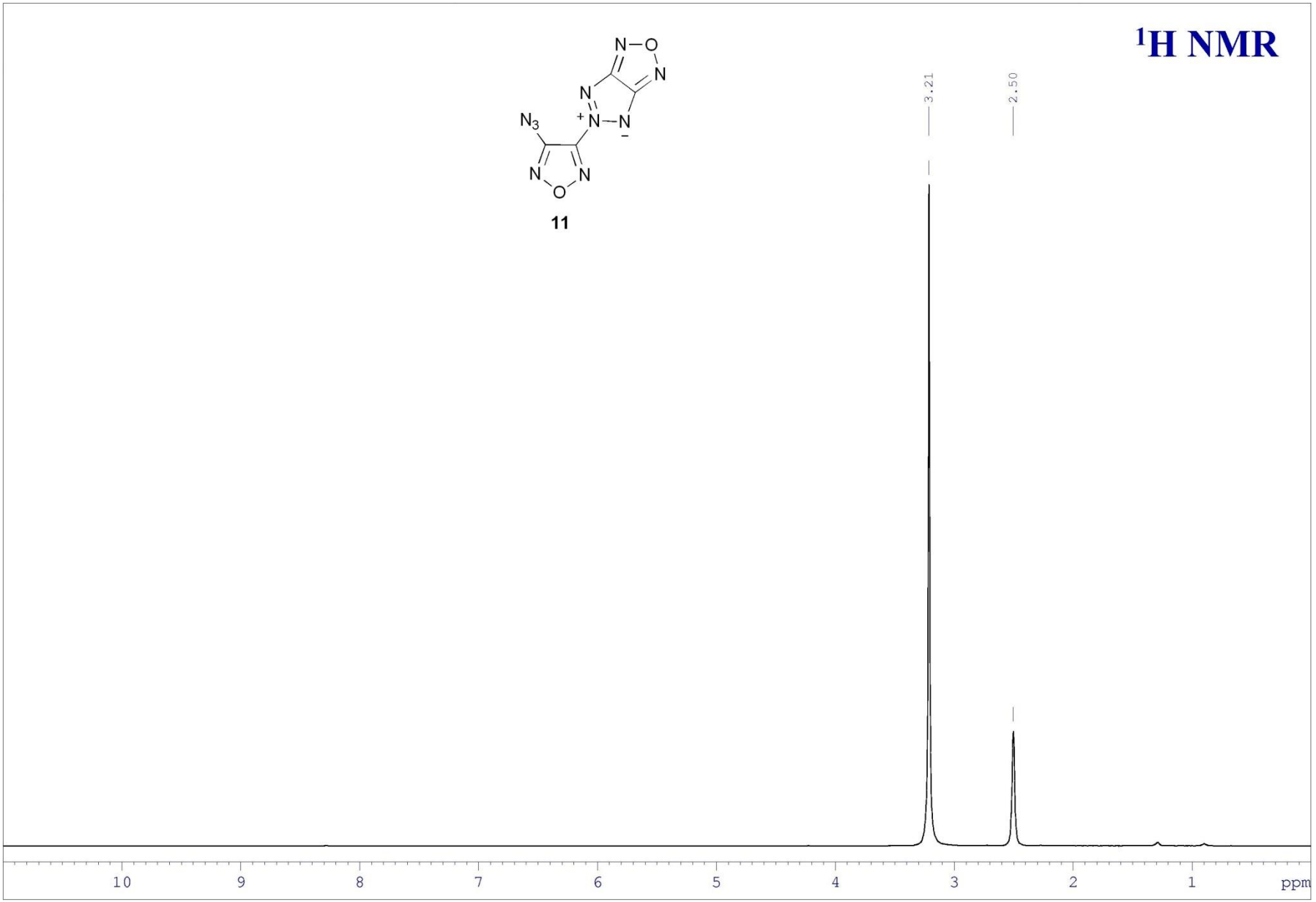

11